公 益 財 団 法 人

応用科学研究所
令和４年度研究成果報告書

第 30 号

RESEARCH REPORT

No.30

2023

RESEARCH INSTITUTE FOR APPLIED SCIENCES

目　次

研究員による成果

鉄鋼材料の超多点硬さ測定・残留歪み測定と材料特性に関する研究

材料評価・開発研究室　長江正寛

１．目的

近年、コストカットへのさらなる要求と材料調達のグローバル化により、同一規格の鋼種であれば可能な限り安価な材料を求めようとする傾向が強まりつつある。しかしながら、それに伴い、歯車等の重要機械部品に関して、材料の品質に起因すると考えられる損傷事故が増えているのも事実であり、購入した鋼材の品質検査の重要性が高まっている。こうした背景から、我々は、数百～数千点のビッカース硬さを短時間で測定可能な「超多点自動 HV 硬さ測定装置」を開発し、超多点のマイクロビッカース硬さ測定は、鋼材の実用特性に影響しかねない組織、合金成分分布などの不均一性を顕在化し、素材や熱処理の良否の判断や、機械部品の損傷原因の推定に対して有益な指針を与えることを明らかにしてきた。また、X 線回折を用いた残留応力測定時に取得されるデバイ環形状のバラツキを評価する目的で、ポータブル型 X 線残留応力測定装置を連続多点自動測定出来るように改良し、鋼材品質との関連を明らかにする研究にも取り組んでいる。

今年度は X 線回折による多点残留応力・半価幅測定を行い、鋼材の旧オーステナイト粒径の違いがデバイ環形状のバラツキにどのような影響を与えるかについて検討した。

２．成果の一例

(1)損傷した大型ベベルピニオン歯の調査から得られた知見

図 1 は浸炭焼入れされた 18CrNiMo7-6 製の大型ベベルピニオン断面の残留応力分布測定結果と旧オーステナイト粒観察結果である。浸炭焼入れ硬化層内には引張の残留応力が生じている箇所が存在する。デバイ環の形状は凹凸が激しく不均質であり、何らかの結晶配向が生じていることが示唆される。ピクリン酸系の腐食液を用いて旧オーステナイト粒観察を行ったところ、100～200μm 程度の大きさの旧オーステナイト粒が至る所に認められ、300mm 程度の粗大旧オーステナイト粒も存在していることが明らかとなった。一般的に、正常な状態の旧オーステナイト

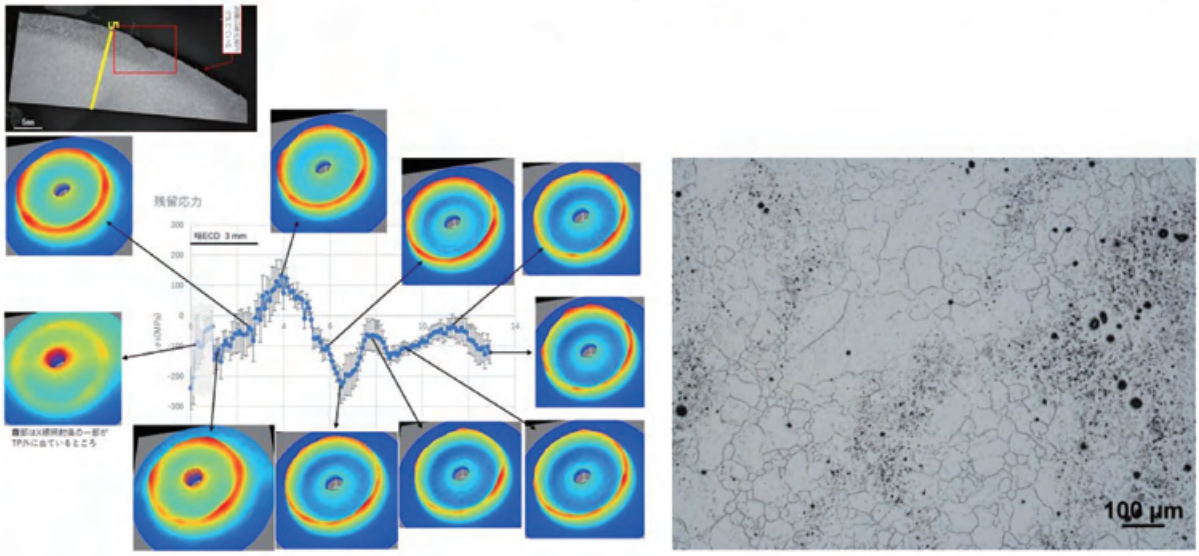

図 1 浸炭焼入れされた 18CrNiMo7-6 製の大型ベベルピニオン断面の残留応力分布測定結果と旧オーステナイト粒観察結果

粒径が 20～30mm 程度であることを考慮すると、この様なオーステナイト粒の著しい粗大化が損傷の引き金となった可能性が高い。オーステナイト粒が粗大化した状態でマルテンサイト変態が起こると、同じような結晶方位を有するマルテンサイトバリアントの割合が増える結果、図 1 に見られるようなデバイ環形状の乱れが生じると考えられる。

(2)異なるメーカー2 社の SCM420 浸炭焼入れ材の比較

図 2 は異なるメーカー2 社の SCM420 浸炭焼入れ材の旧オーステナイト粒観察結果と X 線残留応力測定におけるデバイ環のピーク強度分布である。A 社、B 社材の平均オーステナイト粒径はそれぞれ 26μm、76mm であるが、B 社材では局所的に 500μm を超える粗大旧オーステナイト粒が認められる。デバイ環ピーク強度のバラツキ幅にはその差が顕著に現れており、X 線回折によるデバイ環形状計測を行う事で、複雑なエッチング処理を行うことなく旧オーステナイト粒の粗大化を検出できる事が明らかとなった。

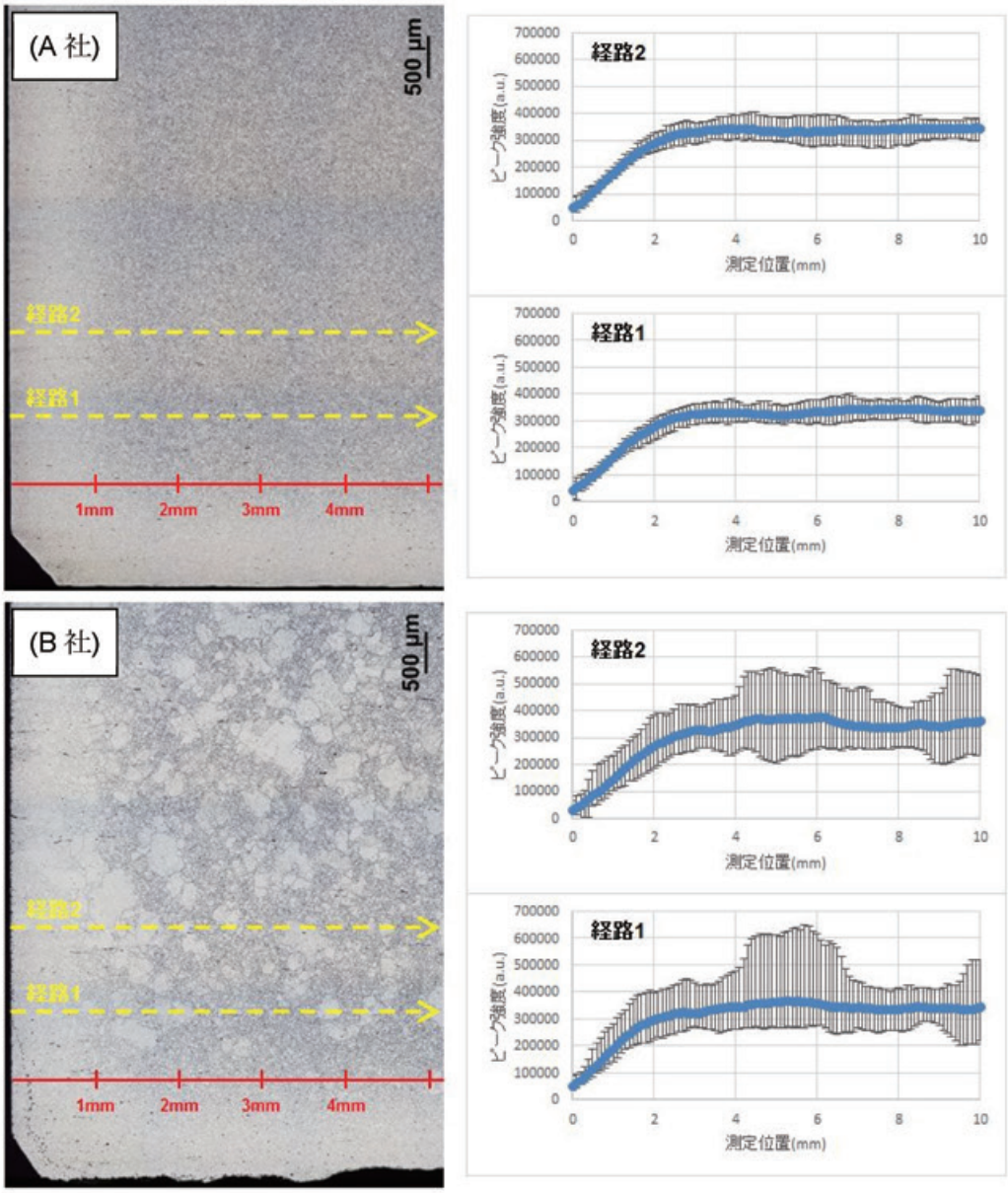

図 2 異なるメーカー2 社の SCM420 浸炭焼入れ材の旧オーステナイト粒観察結果とデバイ環ピーク強度分布

報告書作成日　令和 4 年 4 月 19 日

大強度粒子加速器標的材として採用可能な超耐熱タングステン合金の製造法に関する研究

材料評価・開発研究室　長江正寛

科学研究費助成事業（基盤研究 B）（研究分担者として参加）

1. 目的

宇宙の起源や物質生命科学の解明を目指す大強度高エネルギー陽子加速器では、J-PARC COMET 第二期計画、J-PARC MLF 第二標的計画、米国フェルミ研究所 Mu2e 計画、欧州 ESS 中性子源計画などに代表されるように、中性子発生源である標的材料として高融点金属の一つであるタングステンが期待されている。高エネルギー陽子が標的材料に衝突する際には大きな熱が発生するため，標的材料には耐熱性や熱衝撃耐性も要求される。しかしながら、容易に調達が可能な純タングステンは、高温に曝されると再結晶化による脆化が起こるばかりでなく、高エネルギー陽子の照射による照射脆化の課題も抱えている。

本研究では、東北大の栗下らにより開発され、高エネルギー加速器研究機構に引き継がれた高強度・高靭性 W-TiC 合金の作製法を更に発展させることによって、W-TiC 合金よりも耐熱性に優れ、再結晶脆化・照射脆化の課題を解決し、従来の純タングステンと比較してビーム受入強度を飛躍的に高める W-MC 合金(M は Zr、Ta 等)を完成させることを目的とする。

2. 成果の一例

本年度は W-TaC 系合金の TEM 観察を行った。W 粉末に TaC 粉末を添加し、メカニカルアロイングによって Ta と C を W に強制固溶させた後、HIP 焼結を行い W-TaC 系合金焼結体を作製した。得られた焼結体から厚さ 0.1mm、直径 3mm の TEM ディスクを切り出し、電解研磨によって TEM 観察用試料を作製した。

図 1 に W-3.3%TaC 合金の STEM 像および元素マッピング結果を示す。約 0.1mm から 0.2mm の粒子が W 中に分散しており、元素マッピングの結果、これらの粒子からは Ta, Ti, O, C が検出された。本研究では、W 中に TaC を微細分散させることを目的としているが、合金粉末調整から HIP 焼結に至る過程のいずれかの工程で酸素が混入した事が確認された。Ti はメカニカルアロイングを行う際の容器材料(Mo 系の TZM 合金)からのコンタミであり、現状では避ける事が困難である。HIP 焼結時に再析出した粒子は Ta-Ti-O-C 系の酸炭化物であると考えられ、酸素量低減のためには製造工程の再検討が必要である。

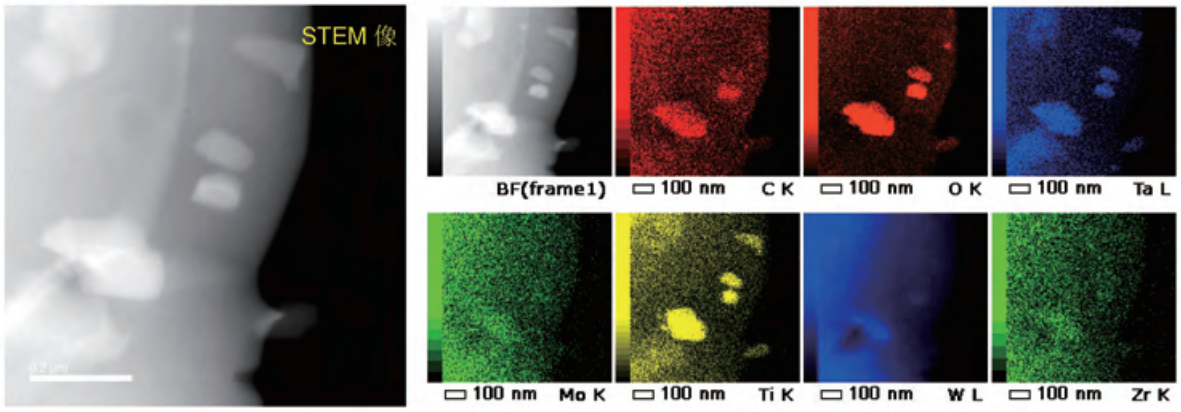

図 1 W-3.3%TaC 合金焼結体の STEM 観察結果

図１において、Ta と Ti が検出されているにもかかわらず、O と C が検出できていない領域がある事が分かる。この原因を明らかにするために、別視野において試料の表側と裏側について同一箇所の STEM 観察・EDX 分析を行った。図２上段が表側から電子線を入射した時の結果であり、下段が裏側から電子線を入射した時の結果である。図１と同様に、Ta-Ti-O-C 系の酸炭化物が分散していることが分かるが、表側入射の STEM 像中赤矢印で示した析出物に着目すると、Ta と Ti が検出されるにもかかわらず、O と C は検出されていない。試料を裏返して観察・分析した結果(下段)、表側からの観察結果とは異なり、赤矢印で示した析出物からは O と C が検出されていることが分かる(上段とは左右が反転している事に注意。これらの結果から判断すると、表側からの視野で見た時、赤矢印で示した析出物は電子線照射面の裏側に露出した粒子であり、その様な粒子から発生する O、C の特性X線は、低エネルギーであるために、マトリックスである W に吸収されて検出されないことが明らかとなった。この結果は W 合金の EDX 分析結果を正しく解釈する上で重要な意味を持つ。

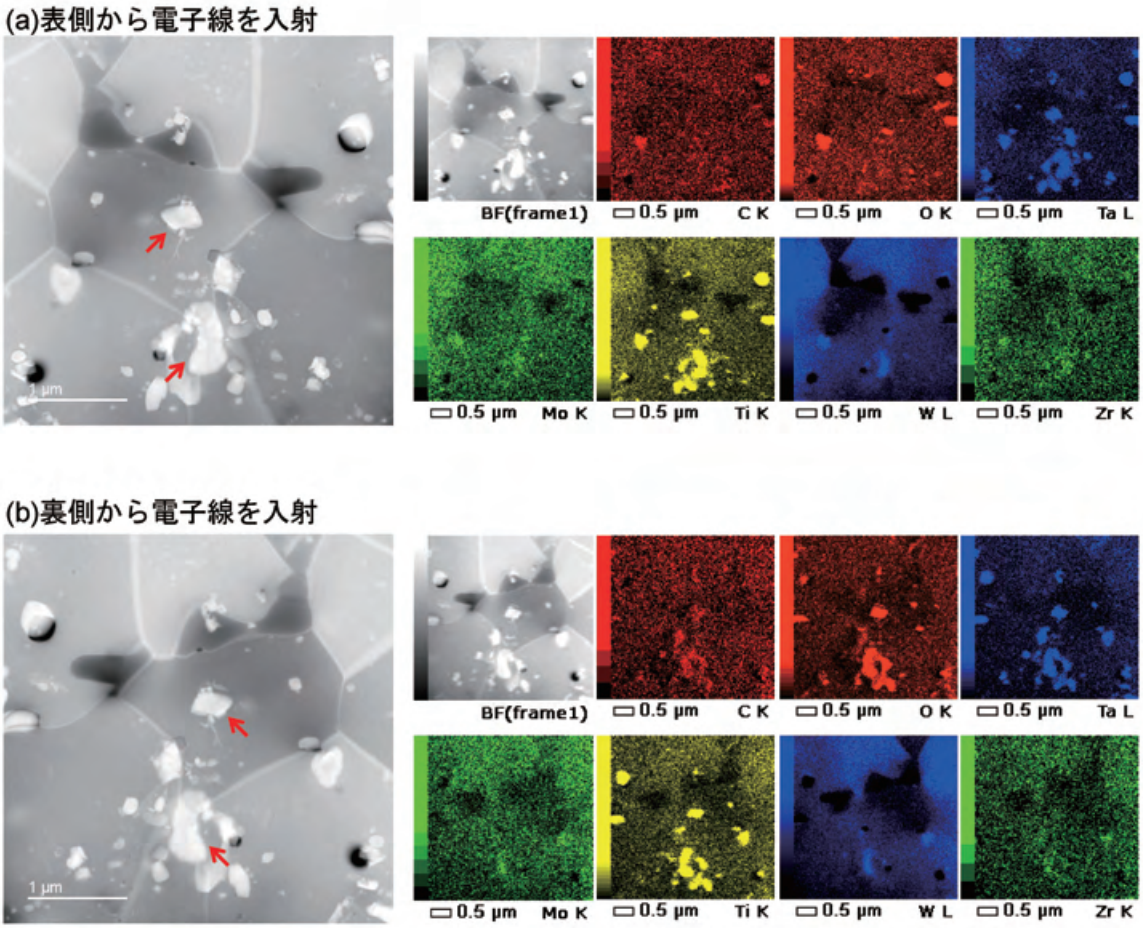

図２ W-3.3%TaC 合金焼結体の STEM 観察結果
(上段：表側から電子線を入射　下段：裏側から電子線を入射)

報告書作成日　令和５年４月７日

機械基盤研究施設からの公表論文

機械基盤研究施設長　久保　愛三

令和4年度は、下記の発表があった。

International Conference on Gears 2022 における研究発表論文

1. 基調講演

Demands in gear technology in structure change of economy

A. Kubo, RIAS (Research Institute for Applied Sciences), Kyoto

別紙参照

2. 発表論文

Development of IP-bevel gears for industrial operation

A. Kubo, RIAS (Research Institute for Applied Sciences), Kyoto

A. Ueda, AMTEC Inc., Osaka, Japan

R. Uehara, H. Ishiyama, DMG/MORI Co. Ltd., Tokyo

別紙参照

3. 発表論文

High-speed measurement of hardness distribution with X-ray diffraction

A. Kubo, RIAS (Research Institute for Applied Sciences)

M. Nagae, RIAS Kyoto, 606-8202, Japan

別紙参照

報告書作成日　令和5年4月3日

Demands in gear technology in structure change of economy

I believe gears are necessary for the fundamental part of driveline technology, independently from the change of primemover such as from ICE to E-motor, or from the change of social and economy structure such as from inflating nature to sustainable nature.

KBGT (Kubo's Gear Technologies)
Research Institute for Applied Sciences
Guest researcher of the FZG from 1972 to 1973.

Aizoh KUBO, Prof.hc.Dr.-Eng.

The meaning of "high performance" in gear technology:

1. High strength, high durability & reliability
2. Good noise and vibration characteristics
3. High efficiency at power transmission
4. Small in size and light in weight
5. Low production cost

We are now saying, the direction that the world should go is toward a sustainable society.

The right figure shows the economic situation of each country from the later half of the 20th century to the first half of the 21st century. The economies of all countries in the world are inflating, and it is obvious they do not aim for a sustainable society.

The only exception is Japan:
Japan has been left behind economically.
However, from a different perspective, Japan has long since outgrown the inflating economy.

In such situation though, Japan has now a huge amount of problems. Do Japanese people feel happy now in such sustainable economical situation ?

The motive force of all human activities is fulfillment of desire, and the judgment of the results is surely based on a comparison of the target matter with the database in the brain of each person that is made by his/her experience.

The biggest subject to realize a sustainable society is therefore, how man feel satisfaction in that society.

There are something for machine engineers to make people happy in the society.:
People feel happy when the machine they use works always in order. Gear technology lives in such atomosphere.

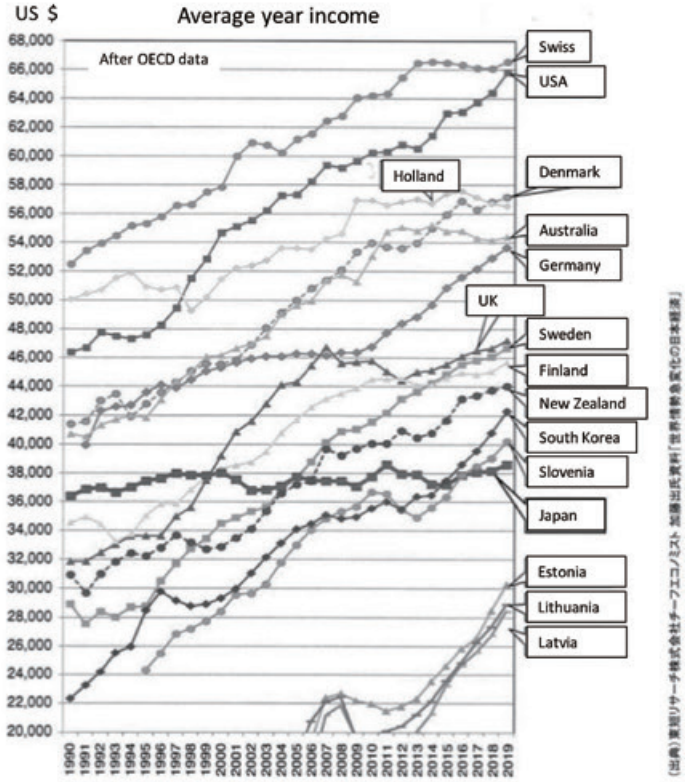

The economy since 19C. was and is of inflating structure -- mass-production and mass-consumption --

The desire of human is endless and it could inflate to destroy the earth.
People has found that the earth is not large enough to permit the infinitely large size of desire.

- Problem of temperature increase due to CO_2 emission
- Problem of water and air contamination
- Disappearing of woods and bees
- Shortage of clean energy and the problem of the lack of its supplying stability

The world tries now to change its structure from **inflating economy nature** to **sustainable nature**, but it is very difficult, because the origin of human activity is to fill their desire !

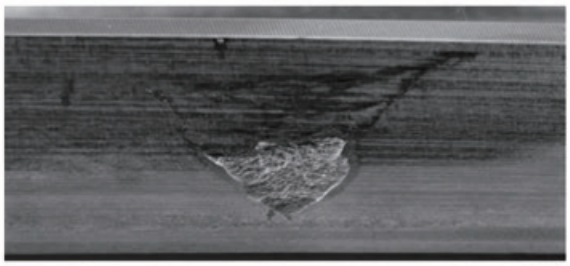

In such the world, can gear technology work to improve the quality of human life ?

Transportation is needed without question for human life and it needs gears. What gear technology is then demanded in such atmosphere ?

➡ Reliability and comfort of transportation, i.e. the reliability of gears and softer NV performance

Many people say, it is fatigue failure of tooth flank, but it is not true.

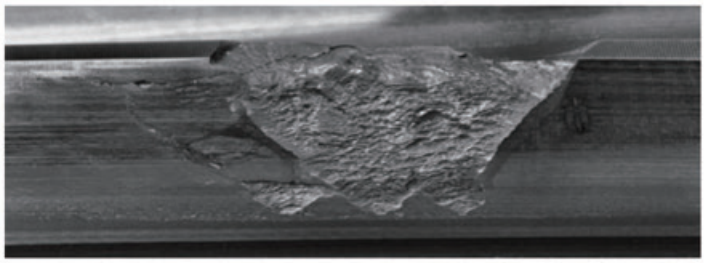

Some examples of unsolved problem in gear reliability today, i.e. failure that today's method for tooth flank durability calculation cannot predict

Attack of tooth tip edge of driven gear to the low limit of the dedendum of driving pinion is the trigger of such failure.

Trochoidal interference during power transmitting gear operation

Explanation for the state of in-mesh situation

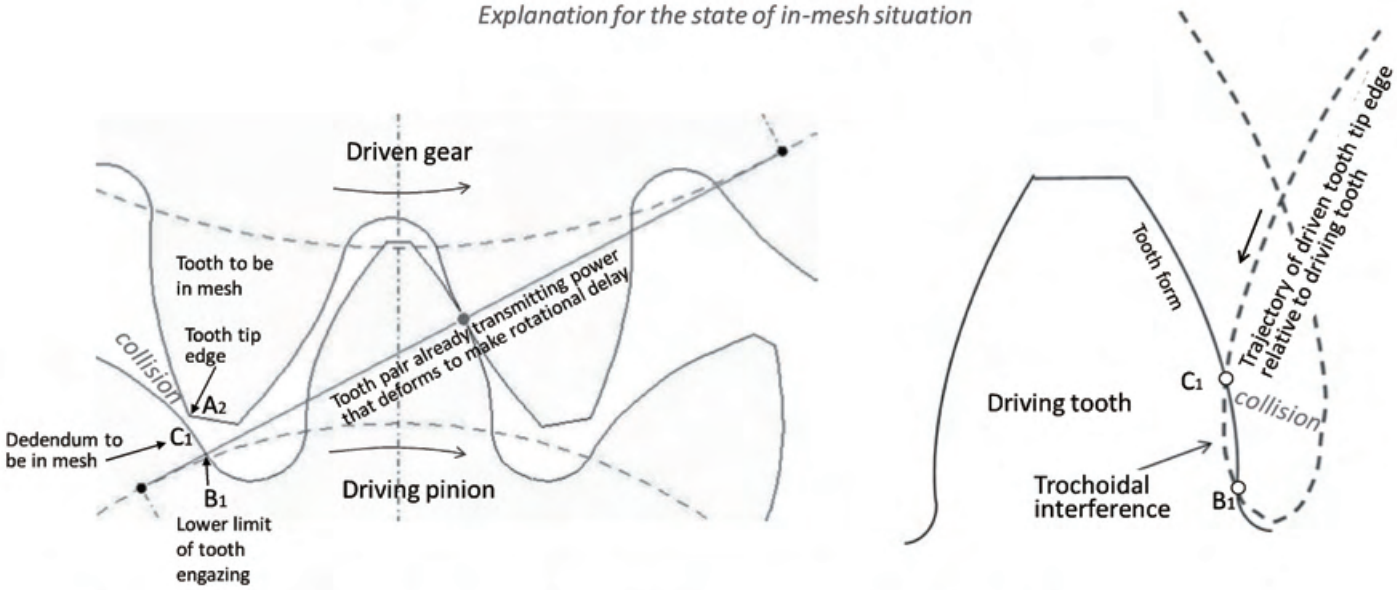

Due to the deformation of tooth pairs already in mesh, the newly coming tooth tip edge of driven gear collides and cuts the dedendum of driving pinion to make interference zone.

State of tooth contact at mesh begin and at mesh end

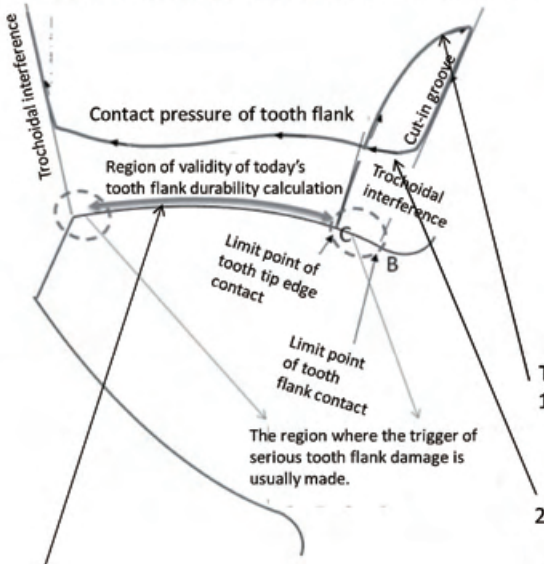

State of trochoidal cut-in region on dedendum

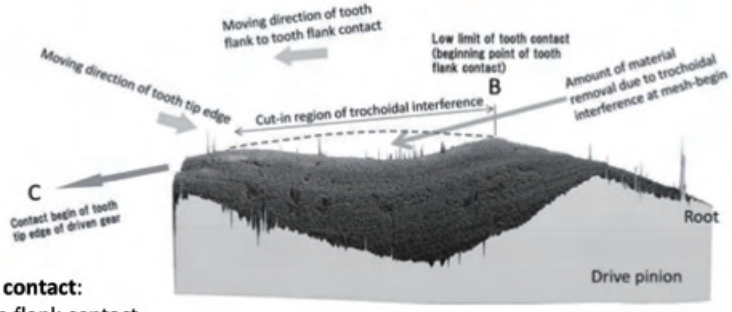

Two times contact:

1st. Edge to flank contact to cut-in the dedendum

2nd. Flank to flank contact occurs as standard gear theory shows

Cut-in groove on dedendum of driving pinion made by trochoidal interference

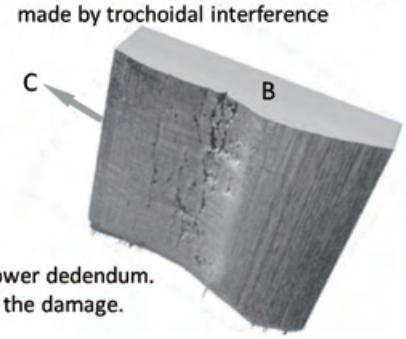

All the prediction methods of tooth flank load carrying capacity deal only with "tooth flank to flank contact" during gear operation.

The most of tooth flank failure of case hardend gear though does not initiate there, but at lower dedendum. In reality, tooth edge-contact occurs during operation and that makes microcracks to trigger the damage.

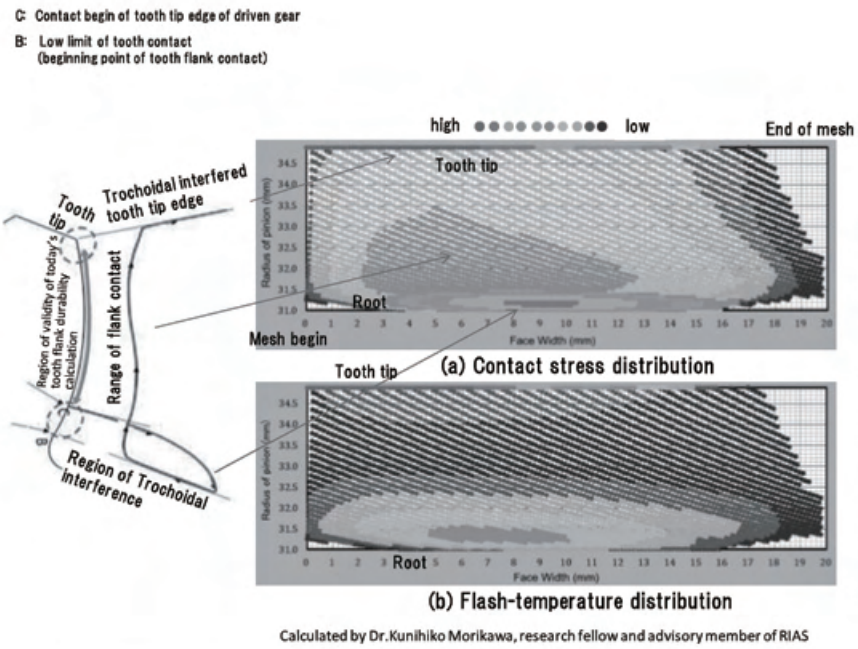

Contact stress and flash-temperature distribution on the plane of action

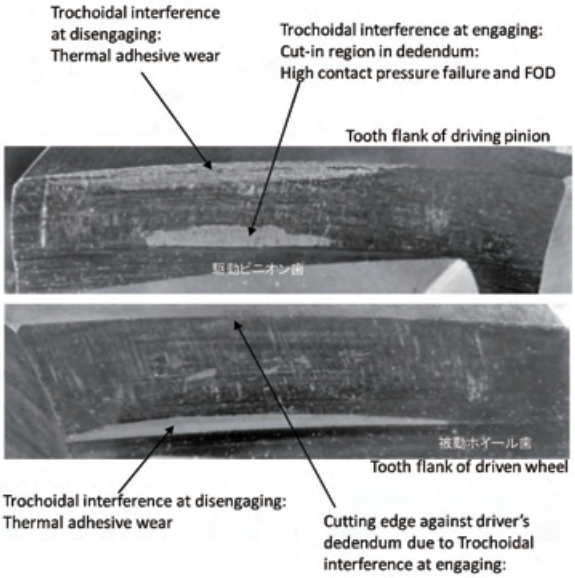

Formation of worn zone due to trochoidal interference that would trigger the peeling-off failure of tooth flank

In the cut-in region of trochoidal interference zone, often pits are found.

From distant view, those pits looks like normal fatigue originated pits, but close observation shows they are mostly the traces of the crash of intruded foreign objects, e.g. wear debris, between meshing tooth flanks, FOD.

Such crash induces often microcracks to trigger failure.

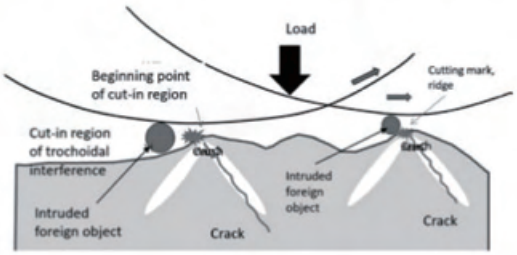

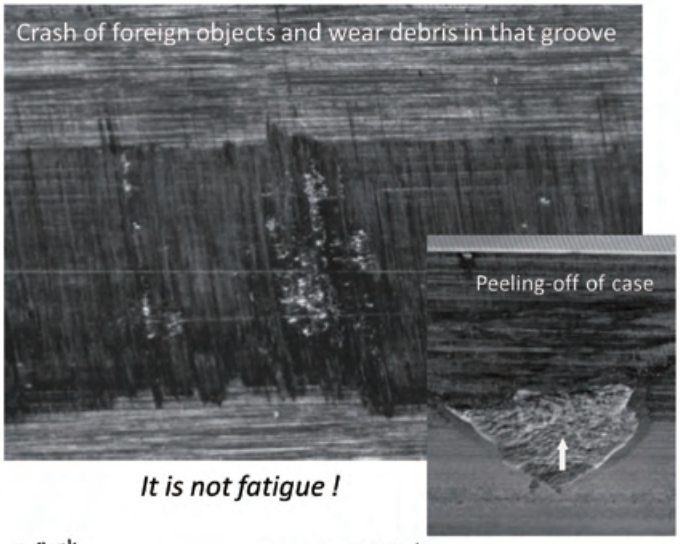

It is not fatigue !

Flaking failure or peeling-off of tooth flank develops from such microcracks at crash of foreign object as shown in the right figure:

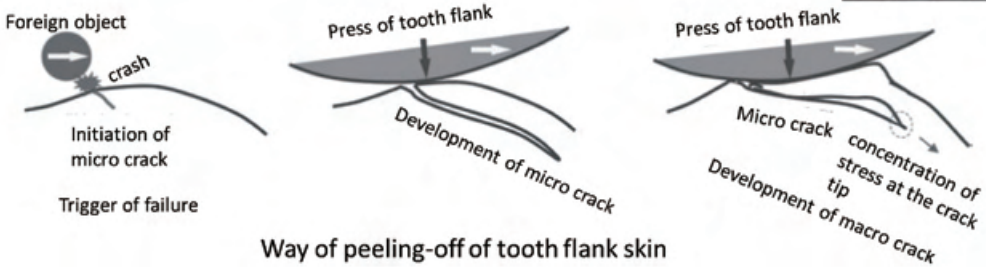

Way of peeling-off of tooth flank skin

When a tooth flank has normal lead crowning and transverse tooth form correction,

Strong edge contact　　No load distribution

Strong tooth flank to flank contact

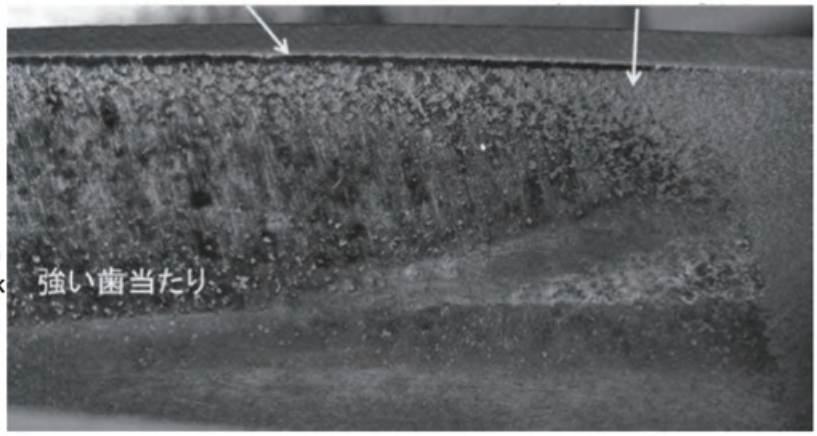

before disappearing edge contact, the load sharing on addendum near tooth tip decreases and the total load carrying capacity of this gearing decreases.
To solve this problem, the transverse tooth form correction must be done after 5th to 7th exponential curve.
This work needs though much labour with conventional gear manufacturing facilities and incorporated only for aerospace gearing.

The research subjects to escape from such gear failure is:

- Tooth edge eliminating technique
- Heat treatment to soften tooth edges lower than the hardness of tooth flank at low dedendum
- Wear debris free gear operation in lubricating oil
- Eliminating method of foreign objects in lubricating oil

Other development requested for high-performance gears are:

- Checking method not to buy poor quality gear steel
- Residual life prediction of gears
- Further progress of gear production method

➡ In today's inflating structure of economy and in foolish political situation over the world, no one invests much money to solve these problem, because such work does not connect directly with the majority of human greed.
To get away from human greed means that the state of economy will become worse.
Those situation makes technical improvement of mechanical engineering difficult.

In human history, greed has made civilization and culture and excess greed has made war, that has made destruction and disaster of happy human life.
As old Chinese wise said, "Goodness exists always in the middle state between too little and too much".
To have too much is far more harmful than to have too little.
Today SNS realizes easy exchange of information between all kinds of people and at the same time, it destroys human relation and the work of human brain.　　*Danger !!*
To think about such problems concerning human happiness, we have to understand the fact that the 1/3 of human population is good, the 1/3 is bad and the rest 1/3 is opportunists as if it were the rule set by Got.

The key is whether we can live more humble with feeling of happiness, or not.
Every religion has taught us this content since over 3,000 years, but in vain.　　*Difficult, difficult !*

In the changing atmosphere of economic structure today, to produce gears of long life will contribute for good human life.
They are demanded now and also in the future, where the world stands on sustainable economic structure.

Ende

Thank you very much for your attention

Key topics:

- Improved simulation methods
- Lubrication for enhanced efficiency
- Condition monitoring with smart gear system
- Multi-body simulation and NVH prediction
- Improved calculation methods for strength and efficiency

Gears interactive

GearArena
Speakers meet up
FZG lab tours
Poster exhibition
Two gear community nights

2nd Conference day
Tuesday, September 13th, 2022

Lecture Room C

Bevel and hypoid gears

Moderation: Prof. Dr.-Ing. Michael Weigand, TU Wien, Austria/ **Prof. Dr. Eng. Ichiro Moriwaki,** Kyoto Institute of Technology, Japan

Development of IP-bevel gears for industrial operation

- Gear features in design and manufacturing
- Performance in transmission error and in load carrying capability

Prof. h. c. Dr.-Ing. Aizoh Kubo, General Manager, Research Institute for Applied Sciences, Kyoto, Japan; Dr.-Ing. Akio Ueda, President, AMTEC Inc, Osaka, Japan; Dipl.-Ing. Hiroya Ishiyama, Productengineer, DMG/MORI Co. Ltd., Iga, Japan

Development of IP-bevel gears for industrial operation

A. Kubo, RIAS (Research Institute for Applied Sciences), Kyoto;
A. Ueda, AMTEC Inc., Osaka; Japan
R. Uehara, H. Ishiyama, DMG/MORI Co. Ltd., Tokyo;

Abstract

To find the potential of IP-bevel gears in practice, the measurement of the transmission error was carried out. The transmission error of IP-bevel gears is as same as that of well-developed automotive bevel/hypoid gears. We improved the dimensions of IP-bevel gears for drive-train of land construction vehicle and carried out the endurance test. The endurance test showed any serious sign of failure to come. We found though slight pits on the dedendum near the big end of driving pinion at the beginning point of tooth meshing due to the attack of tooth edge of driven wheel. New method to rounding-down the tooth tip edge form as 3D-modification is proposed to prevent such tooth flank failure triggered by the trochoidal interference under heavy duty operation.

1. Introduction

In the field of big bevel gear production, incorporation of 5 axis controlling machining/ grinding station (refer to 5X machine) becomes usual. The biggest problem of such bevel gear production with 5X-machine is the low productivity in comparison with specialized dedicated bevel gear producer like Klingelnberg's or Gleason's machine (refer to conventional machines). The reason of this is, (1) many paths of the cutting tool movement are necessary to generate 3D curved form of tooth flank, and (2) simultaneous machining or grinding of both tooth flanks, i.e. front and back flank, at the same time is impossible. To raise the production rate of bevel gears with 5X-machine, authors invented IP-bevel gear whose larger wheel has flat tooth flank for easy production and the pinion has the conjugate 3D tooth flank form to that flat tooth flank of the wheel[1]. The demerit (2) above can though bring considerable merit in the gear performance at actual heavy usage. For example, the edge-eliminating 3D treatment of tooth tip of IP bevel wheel is far easier than that of twisted tooth of conventional bevel wheel. Another merit of IP-bevel gears is that their conjugate teeth mesh is geometrically not as point-contact, but as line-contact on the tooth flanks at power transmitting action. IP-bevel gears have therefore a bigger margin for increasing the load carrying capacity in principle in comparison with the conventional bevel gears whose teeth mesh is geometrically as point-contact.

2. Transmission error

Soft gear noise and vibration during operation is very important factor in practical usage of gearing. We have to find, whether IP-bevel gear has the nature for the merit in noise and

vibration generation. LTCA checking machine was incorporated to check the transmission error. The dimension of the test gear is module 6mm, PA 20deg., tooth number 9/33, lead angle 30deg. and face width 30mm, as seen in Fig.1. The tooth contact pattern and the transmission error under 600Nm loading was checked, considering the influence of alignment change, where ⊿P is the

Fig.1 IP-bevel gears used for the LTCA test.

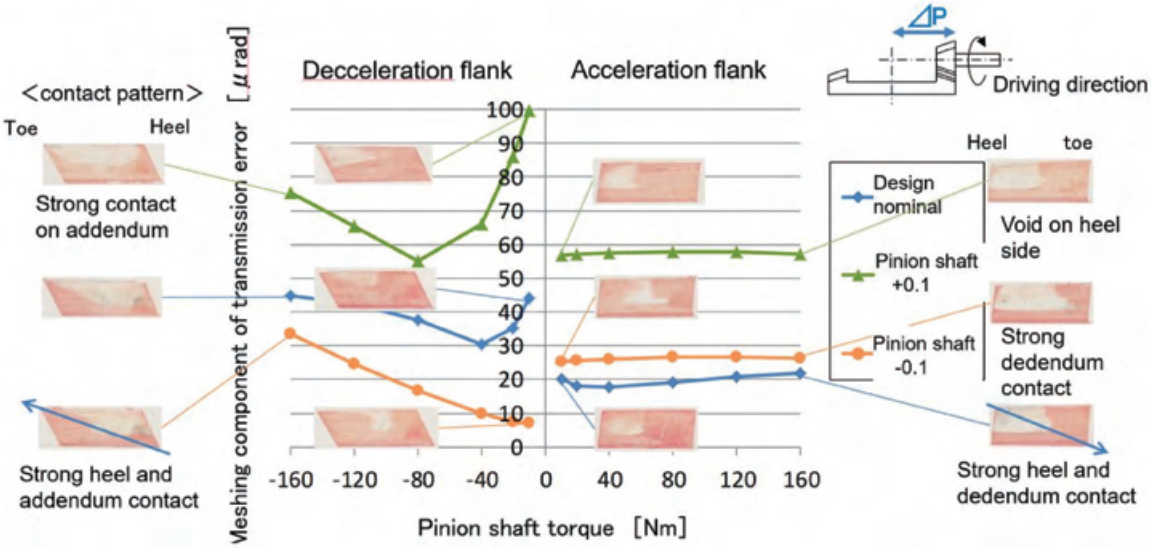

Fig.2 Influence of ⊿P on the transmission error of IP-bevel gears

mounting deviation of pinion, ⊿G is the mounting deviation of wheel and ⊿E is the offset deviation. An example of the result is shown in Fig.2. Among many influencing factors, the influence of ⊿P is the largest. The transmission error at the run of acceleration tooth flank receives small influence from transmitting torque. The transmission error of IP bevel gear can be as small as that of automotive hypoid gears, when tooth contact pattern is adjusted in good state.

Fig.3 shows the example of measured wave form of the loaded transmission error for the acceleration flank run. The result of frequency analysis is also shown. Because of the limitation of pages of this paper, other influences of mounting deviation cannot be shown here, but the rough tendency between the mounting deviation and the transmission error is summarized as follows:

(1) The spreading and moving tendency of contact area on tooth flank is similar to that of the conventional bevel or hypoid gears: i.e. The load carrying area on tooth flank spreads toward big end, when the tooth flank load increases.

(2) The moving direction of the contact area due to mis-alignment, or to mounting deviation ⊿P, ⊿G and ⊿E, is similar to that of the conventional bevel or hypoid gears.

(3) The influence of the mis-alignment on transmission error is stronger in the following order: ⊿P > ⊿E > ⊿G.

(4) The magnitude of waviness of the transmission error is almost equal to that of the conventional bevel or hypoid gears.

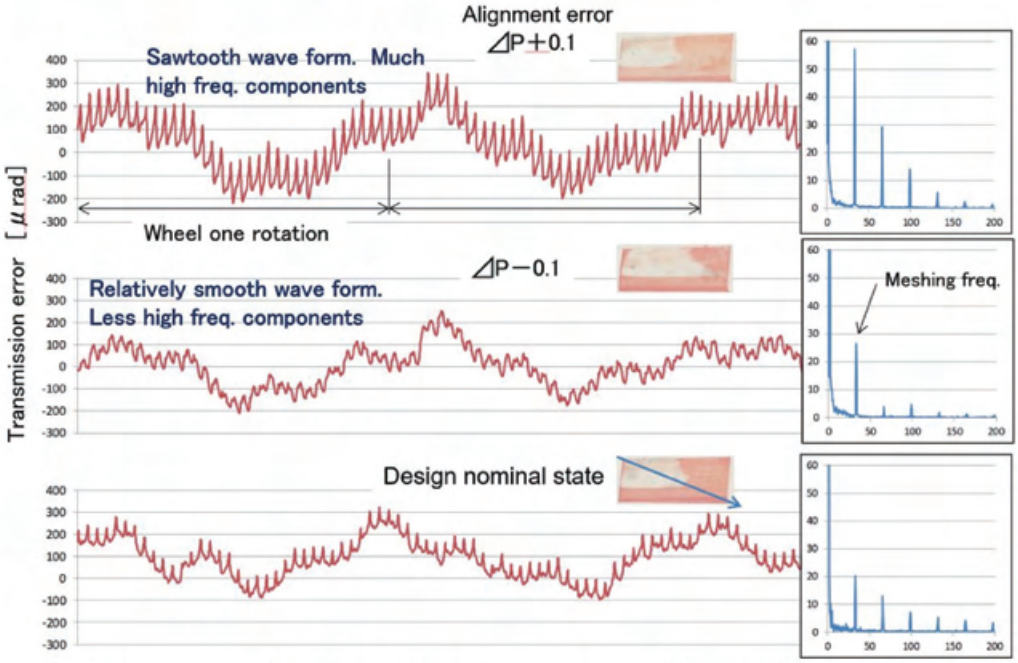

Fig.3 Influence of ⊿P on the transmission error, wave form and the spectrum

3. Improvement of gear design and test rig for load carrying capacity

There are a lot of design parameters for the configuration of IP-bevel gears and we still do not know the optimum geometrical configuration or the recommended gear specification of the IP-bevel gears. To develop the IP-bevel gears for the drive train of land construction vehicle, the gear dimension is improved by using simulation program for gear performance. The gear dimension is listed on Table 1. The outlook of this new IP gear is shown in the right side of Fig.4.

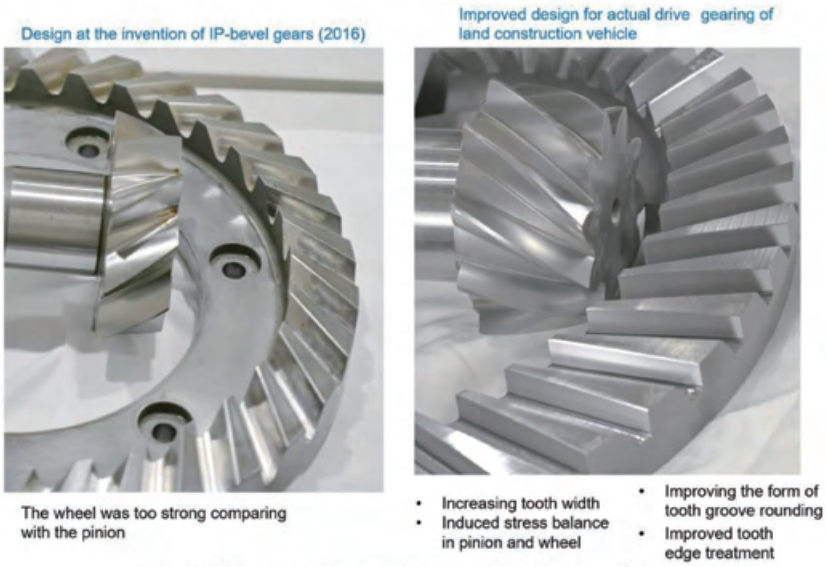

Fig.4 Improvement of geometrical gear dimension

4. Endurance test

This gear set was mounted in the actual gear box used today in the commercial vehicle and was back-to-back tested with rectangular power circulating rig as shown in Fig.5. With this test rig, all the gear boxes are of the same dimension and the bearings are also the same. Only one gear set is changed from conventional bevel gears to the IP bevel gears. As same as conventional bevel gear drive, the alignment of IP-bevel gear set must be adjusted into proper position by checking the tooth contact pattern. Fig.6 shows how the contact pattern changes as function of axial positioning of pinion and wheel shafts. The rigidity of the gear box was already measured and using this rigidity, the proper intended contact pattern at no loading is simulated as shown in the figure and the adjustment of gear mounting was carried out to realize this contact pattern. The simulation indicates that the contact area on tooth flank would move and reach the proper position at the rated loading value. Fig.7 shows the observed state of the movement of contact area, when the transmitting load increases.

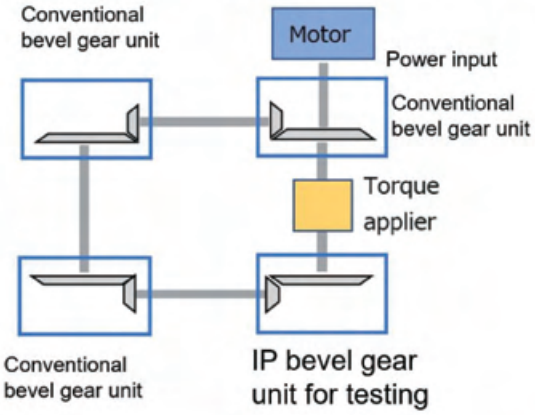

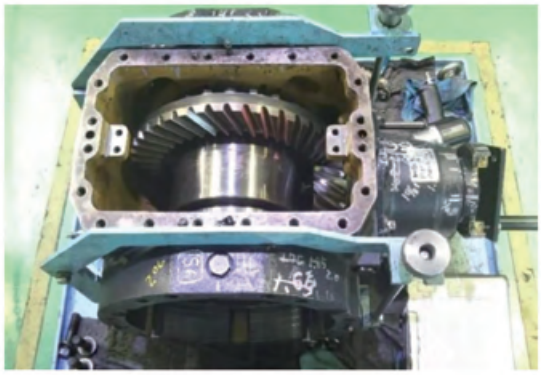

Fig.5 Endurance test rig

Table 1 Gear dimension for the endurance run

Basic item	Symbol	Unit	Pinion	Wheel
Gear tooth shape	---	---	Equal module profile	
Normal module	mn	mm	6.0000	
Normal pressure angle	αn	deg	16.0000	
Teeth number	z	---	10	41
Helix angle(lead angle)	β	deg	38.0000	38.0000
Helix direction	---	---	Right hand	Left hand
Shaft angle	Σ	deg	90.0000	
Dimension item	**Symbol**	**Unit**	**Pinion**	**Wheel**
Addendum	ha	mm	6.5000	
Dedendum	hf	mm	7.5000	
Reference cone angle	φ	deg	13.7070	
Offset	Xo	mm	0.0000	
Rolling circle radius	r	mm	40.0000	140.0000
Gear inside diameter	di	mm	---	290.0000
Gear outside diameter	do	mm	---	400.0000
Pinion inside distance	Js	mm	145.0000	---
Pinion outside distance	Je	mm	200.0000	---
Face width	b	mm	55.0000	55.0000
Tooth thickness	sj	mm	---	10.6814
Normal backlash	Jn	mm	0.6000	
Tip R	ra	mm	1.0000	1.0000
Root R	rf	mm	2.0000	2.0000
Backlash angle	Jθ	deg	0.0599	0.2456
Offset angle	θ	deg	0.0000	
Outside cone distance	La	mm	*****	205.8629
Inside cone distance	Lf	mm	*****	149.2506
Cone angle	δ	deg	13.7070	76.2930
Outward form item	**Symbol**	**Unit**	**Pinion**	
Cone height	b	mm	55.0000	
Inside diameter	Dt	mm	94.0216	
Outside diameter	Db	mm	119.2731	

Considerable big difference was observed in the size growth and movement of contact area between that of IP-bevel gears and that of conventional bevel gears, when the transmitting load increases: The contact area on the tooth flank of the IP-bevel gears spreads easily to cover whole the tooth flank, but it would never be so in the case of conventional bevel gears.

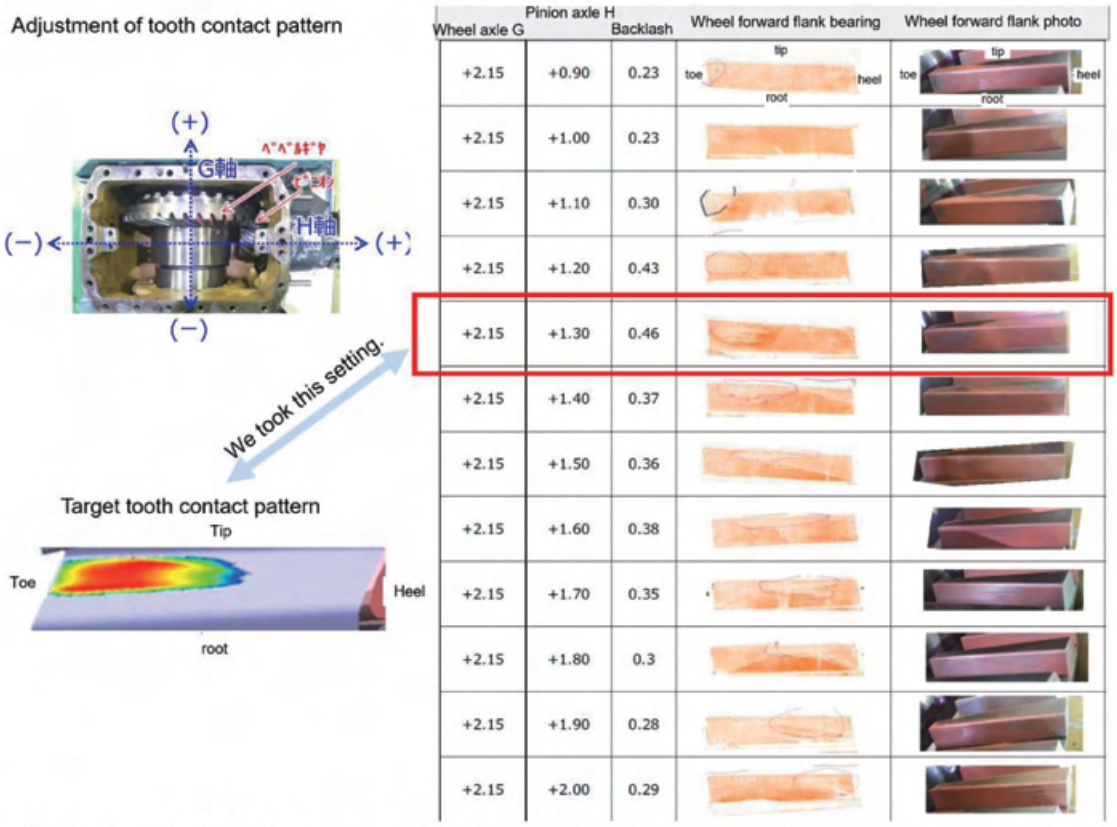

Fig. 6 Change of tooth contact pattern as function of axial positioning of pinion and wheel, and comparison with the simulated target figure.

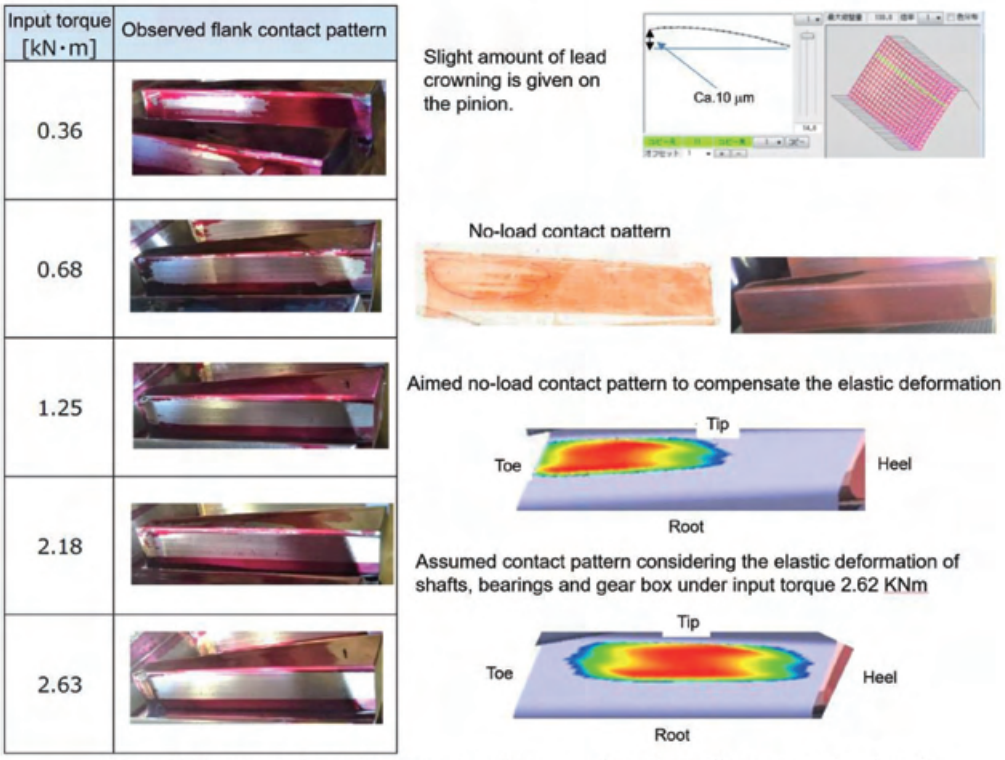

Fig. 7 Change of tooth contact pattern as function of transmitting load

Many years of our experience of land construction vehicle shows, that the life reliability of actual bevel gears operating in fields is guaranteed, when the endurance run of the gearing gets 1,250hrs at 1,600rpm under the pinion shaft torque 2,620 Nm with this power circulating

rig. This driving condition is therefore incorporated for the endurance test of this IP-bevel gear set. When we began the endurance run, we have confirmed that the noise and vibration from the IP-bevel gear box is quite similar to those from the same gear box with conventional bevel gears.

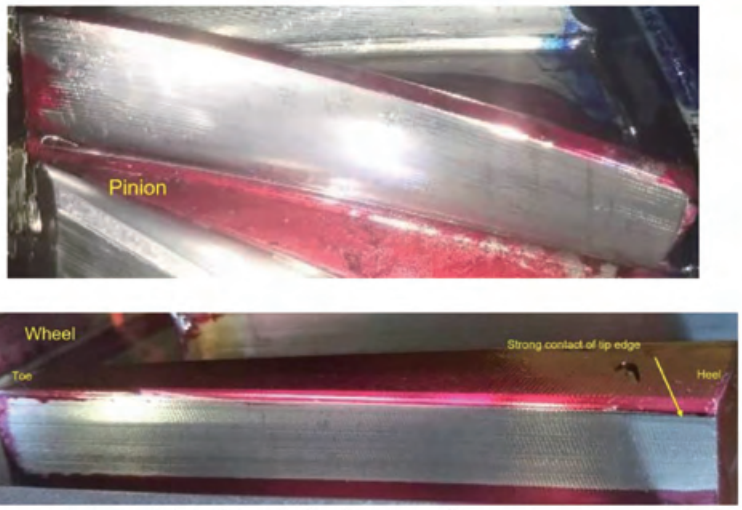

Fig.8 State of tooth flanks after 9hrs run

The observed state of tooth flank after 9 hrs of operation shows that the tooth contact area shifts somewhat toward the heel as same as the tendency of conventional bevel gear drive. The driving tooth flank of the pinion is concave and the tooth flank load pushes the pinion shaft into axial direction. In the region near the toe, tooth flank looks to contact softly, this is due to the alignment change, i.e. elastic deformation of gearbox and pinion shaft induced by transmitting torque. With this endurance run of IP-bevel gears, we confirm also that the contact area on tooth flank easily spreads over the whole tooth flank. Surely it comes from the conjugacy nature of the tooth flank geometry of the IP bevel gears. The tooth tip edge from the middle of face width to the heel of the IP-bevel wheel seems to be somewhat worn or rounded by plastic deformation. This is a proof that the tooth tip edge of the driven wheel has attacked the dedendum tooth flank of the driving pinion at the beginning point of tooth contact at engaging, i.e. the trochoidal interference occurs.

During the endurance run, we scheduled to stop the test rig at regular time interval for investigating the damage state of tooth flanks. Until 1000hrs of the run, no sign of damage initiation was found on the tooth flanks. This is a considerable big difference from the state of tooth flanks of conventional bevel gears: that is, on the center region of tooth flank of conventional bevel gears, the contacting surface shows usually considerable clear signs of scratching, of high temperature and of thin lubricating oil film thickness already at this stage of endurance run. At the beginning place of tooth contact on the driving tooth dedendum, in the middle of face width, usually clear sign of the attack of driven tooth tip edge, i.e. trochoidal interference, is observed. In the case of IP-bevel gears though, such sign was very soft, and it was not observed at the middle of the face width, but at the dedendum near the heel. As the total impression of the observation, we cannot imagine at this stage of the endurance test, how long will the life of this IP-bevel gear tooth be.

At the inspection after 1250hrs of the run, we cannot find any sign of damage on the tooth flank after “flank to flank contact” repetition, but we have found small peeling-off spot of tooth flank

at the contact-limiting position on the dedendum of driving pinion at heel side, surely due to trochoidal interference, and the endurance run was stopped.

Fig.9 Peeling-off spot of pinion dedendum (severest spot)

Fig.9 shows the severest peeling-off spot on the pinion dedendum. We find also the clear strong trace of tooth side edge contact as the vertical line along transverse tooth form. This strong contacting trace at tooth side edge suffers adhesive wear. Uneven load distribution on tooth flank to increase the load distribution near the heel induced such state of strong tooth side edge attack. This uneven load distribution induced also a strong trochoidal interference on the pinion dedendum near the heel. The tooth tip edge of driven wheel attacked the driving pinion dedendum near the heel to make the peeling-off of the tooth flank there. With conventional bevel gears, the same kind of pits are usually observed at the middle of face width, but in the case of IP-bevel gears we cannot recognize any signs of such pit formation at the middle of face width.

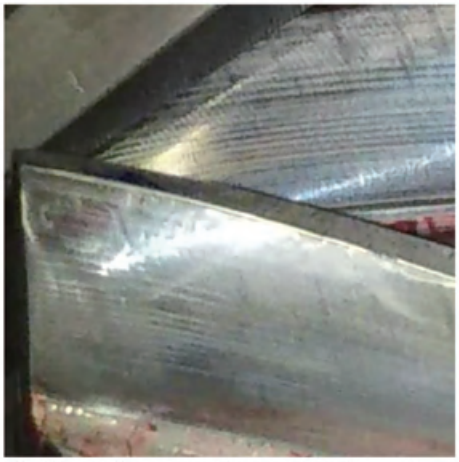

Fig.10 Soft contacting state of tooth flank near toe

Fig.10 shows the state of tooth flank from the middle of face width to the toe. The main part of the tooth flank at the middle of face width shows that this part carries strong load distribution: Some scratching, crash of wear debris and adhesive wear are observed. Slight trochoidal interference is observed at the dedendum, but it is considerably softer than that of conventional bevel gears. The pit formation on the beginning point of tooth contact on the dedendum of the IP-bevel pinion is far from the failure. The flank near the toe shows the appearance that this region carries small load. At the toe side edge of tooth flank, we do not observe any signs of strong contact. No indication of trochoidal interference is also observed on the dedendum near tooth root.

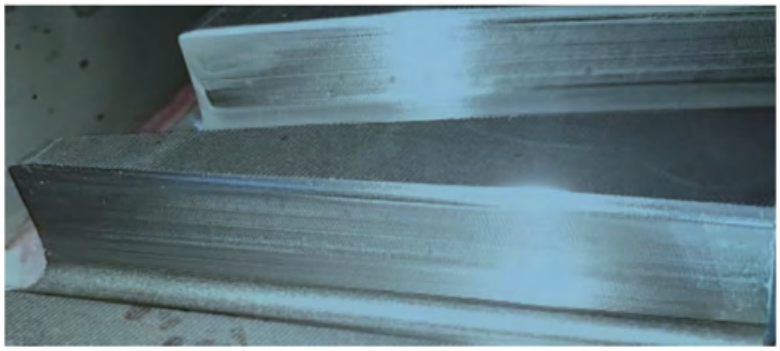

Fig.11 Tooth flank of the wheel

Fig.11 shows the state of the wheel tooth flank. It looks as if it were new. At tooth tip edge from the middle of face width to the heel, we find some outlook of strong contact, that is the evidence that this part of tooth tip attacked the pinion dedendum at the low limiting place of tooth contact.

5. Tooth edge treatment

The state of tooth flanks from Fig.8 to Fig.11 suggests that the elastic deformation of gearbox due to the transmitting load is larger than that we have expected: the amount that we have used in the simulation was too conservative, cf. Fig.7. The induced alignment error shifts the center of load distribution more to the heel side of the teeth. The tooth tip edge of the driven wheel contacts strongly to the dedendum of driving pinion near the heel more than we have expected and this is believed to be the main cause of the failure shown in Fig.9. The gear manufacturing to avoid the tooth edge contact is strongly demanded also for the IP-bevel gears to make it reliable.

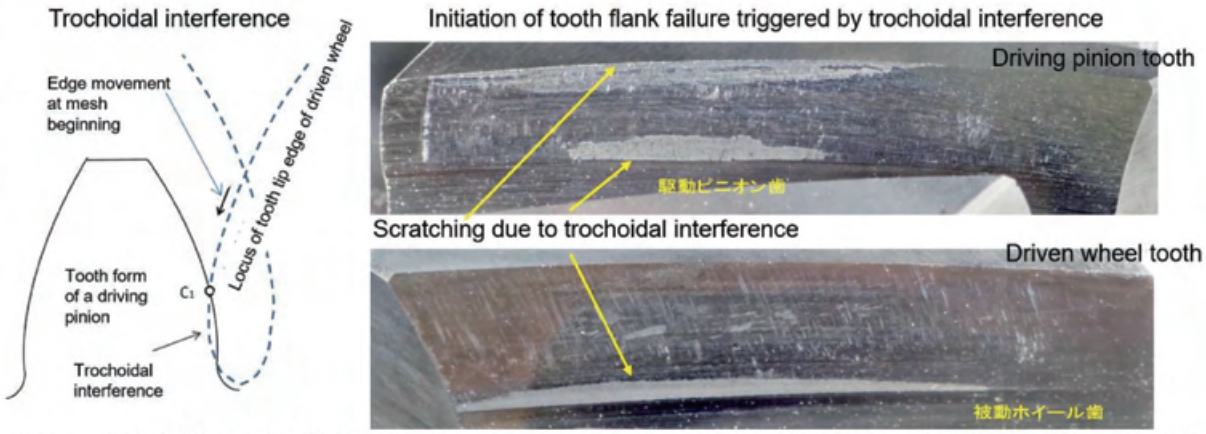

Fig.12 Attack of tooth tip edge against mating tooth flanks (example for a case of involute helical gears)

Fig.12 shows how the tooth tip edge makes the triggering failure of tooth flank. This is in a case of involute helical gears, but the phenomenon is quite same also for bevel gears as shown in Fig.13.

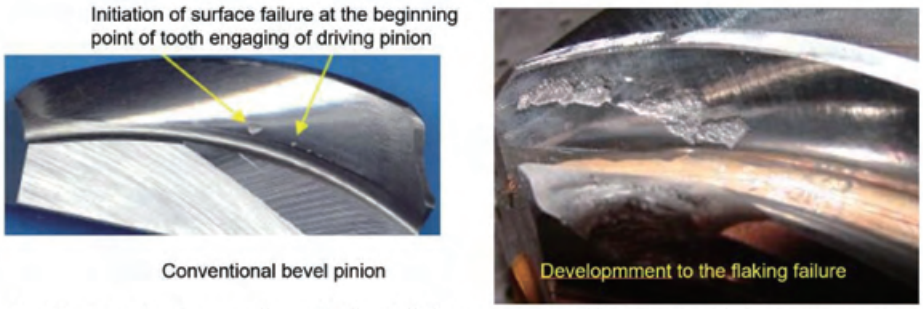

Fig 13 Development of tooth flank failure triggered by trochoidal interference

To avoid such failure, tooth tip edge, especially tip edge of driven gear, must be smoothly rounded down. An example of the target form of the tooth tip rounding in transverse section is shown in Fig.14. To give this corrective tooth tip form is not easy work in gear production with conventional gear manufacturing machines. The IP-bevel gears are though manufactured only with 5X-machine and 5X-machine carries out this job without big difficulty. That is:

1. As the extension of the 3D form generation of tooth flank by milling with 5X-mashine, tooth tip edge is treated as the extension of tooth flank form and is cut as continuous motion of tooth flank generation

2. The tooth tip rounding must have quasi exponential curve, say 500μm from the tooth tip

edge to the addendum flank and 150μm drop in the tooth tip crest for a case of module 6mm gear teeth, cf. Fig.14.

3. To make this curve of tooth tip edge form, the first step is the milling to make the base of the target dimensional figure: As the continuous tooth flank form generation, the milling tool cuts the tooth tip edge region by 3 paths A, B & C, cf. Fig.15.

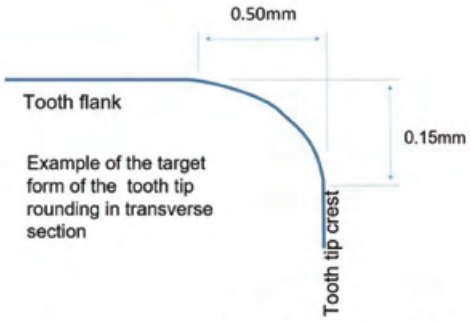

Fig. 14 An example of tooth tip rounding

After the milling of tooth flank and tip edge, secondary edges were born at the tooth tip region. They are the inflection points of tooth flank form between milling path A, B and C.

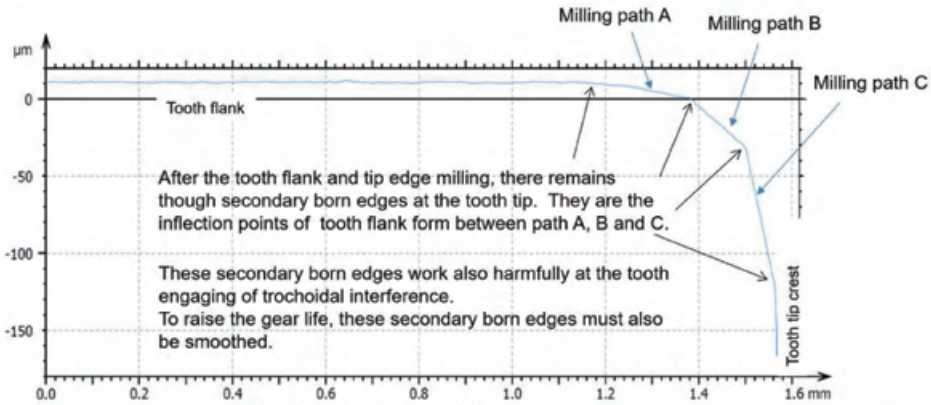

Fig.15 tooth tip milling

Such secondary born edges work also harmfully at the tooth engaging accompanying trochoidal interference.

To improve the gear life, these secondary born tooth tip edges must also be smoothed. For this purpose, we develop new soft elastic grinding disc whose life is longer enough to finish the grinding the total tooth tip length of middle to large size bevel wheel e.g. of m_n=6mm, Z=41 and b=55mm. After the 3 paths of tooth tip milling mentioned above, we change the milling tool to this soft elastic grinding disc and polish-grind the tooth tip with one path. The result is shown in Fig.16. The shape, the amount of rounding drop of tooth tip and the smoothness are all satisfactory to avoid harmful action of tooth tip edge at gear meshing.

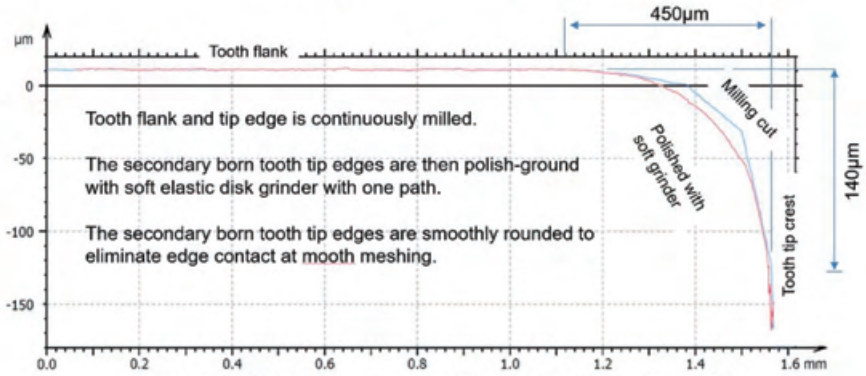

Fig.16 Polished tooth tip edge of intended dimension

When we consider actual gears operating in field, almost all of them have lead crowning of tooth flank micro-form modification. As seen in Fig.12, the amount of trochoidal interference then differs along face width. To avoid harmful action of tooth tip edge at gear meshing due to trochoidal interference, the amount of tooth tip rounding must be changed along face width as function of the amount of tooth lead crowning modification. Such 3D tooth tip rounding is almost

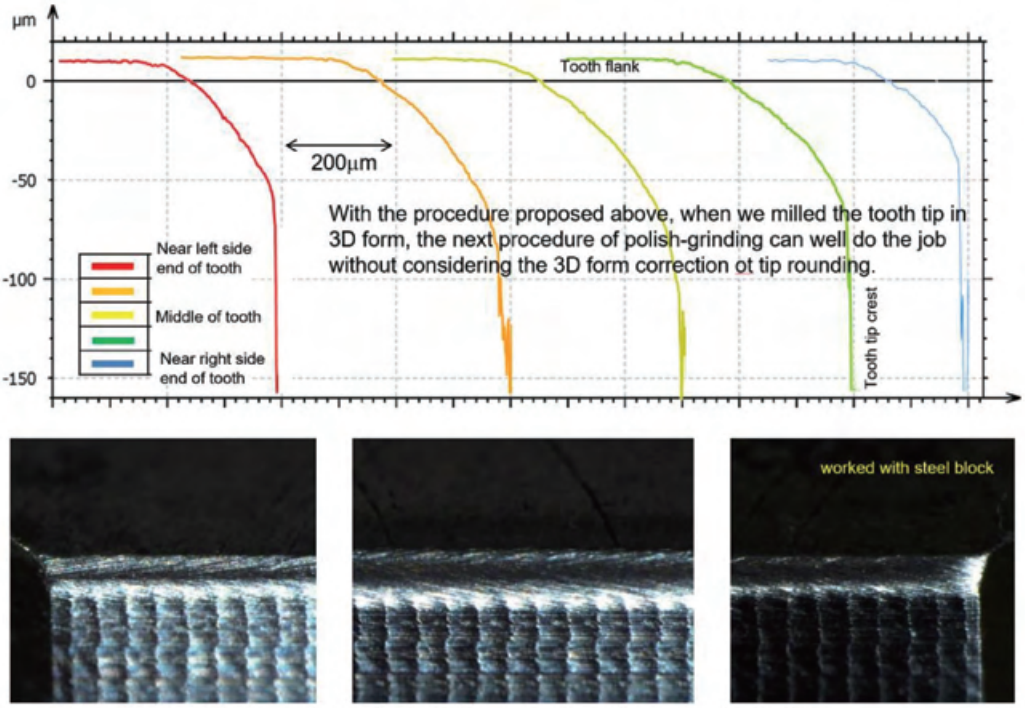

Fig.17 3D tooth tip edge rounding along tooth width

impossible with today's gear manufacturing machines for conventional bevel gear production. In case of IP-bevel gears, they are produced with 5X-machine and 5X-machine can easily carry out such 3D tooth tip rounding without difficulty after the procedure mentioned above. Fig.17 shows an example of such 3D tooth tip rounding along face width.

6. Conclusions

For the industrial incorporation of IP-bevel gears, the performance of the IP-bevel gears is tested in rotational angle transmission error and in endurance performance.

1. The IP-bevel gears show satisfactory small transmission error to bring good noise and vibration performance. The durability is better than that of conventional bevel gears. This means, by incorporation of IP-bevel gears, the increase of gear performance can be achieved together with reduction of gear production time and cost.

2. Trochoidal interference, i.e. the attack of tooth tip edge to the dedendum of mating gear, brings sever problem also with IP-bevel gears as same as the case for conventional bevel gears. With speed reducer, tooth tip rounding of driven wheel is therefore very important.

3. In case of IP-bevel gears, not only the tooth flank form generation, but also the tooth tip 3D rounding can easily be done with 5X-machne as the extension of tooth flank form generation to increase the performance of bevel gear drive. To make smooth 3D tooth tip edge rounding is not difficult.

7. Future possibility for optimum geometrical design of bevel gears

As you well recognize from the photo of IP-bevel gears, the tooth bottom width of IP-bevel pinion and the tooth tip crest width of the wheel near the heel looks abnormally wide. If the addendum height of wheel is extended and the dedendum depth of pinion is engraved deeper as the extension of workable tooth flank, the area of the usable tooth flank near the heel becomes considerably larger. Such extended tooth flanks can well mesh to realize the conjugate action for transmitting power. Incorporation of continuous pressure angle change along the lead from low PA at toe to high PA at heel brings further better result. All those modified IP-bevel wheel can be toothed efficiently with disk-form cutter.

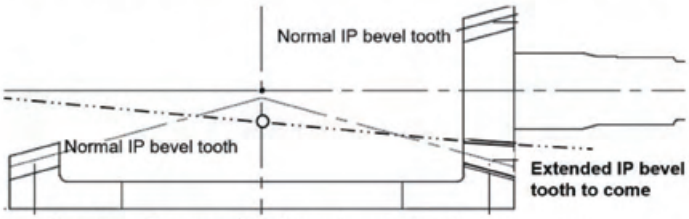

Fig. 18 Future of IP-bevel gear tooth geometry

The experience of the IP-bevel gear production with cylindrical milling tool reveals that the transverse cutting depth of one milling path is usually limited to about the diameter of the tool to prevent a mal-effect of elastic deformation of the tool during the milling process. That means 3 to 4 paths are usually necessary to make even flat tooth flank of large module gear. Because a slight PA change at the change of milling path does not cost the increase of working rate and the convex amount of transverse tooth form of bevel-wheel is usually very small, the generation of convex transverse tooth form of the wheel can be worked out without decreasing the efficiency. Incorporation of one path finishing with soft disk or ellipse grinder as mentioned in Fig.16 after the milling process is possible. That suggests even the generation of spherical involute bevel gear tooth with 3D tooth edge rounding can also be made very efficiently. It is well known that the spherical involute bevel gears bring big merits in its performance comparing with today's conventional bevel gears. The incorporation of spherical involute bevel gears in practical industrial usage is at hand. The demerit of such bevel wheel with curved tooth lead in comparison with the IP-bevel wheel is that the disk-form cutter is difficult to use for working the flank of concave lead.

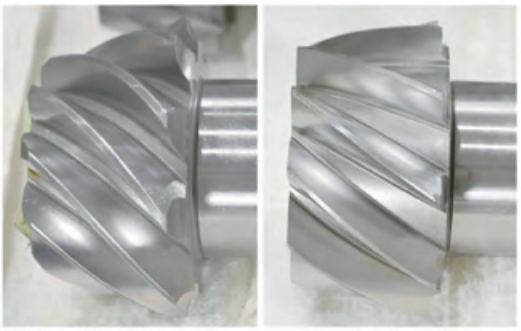
Spherical involute bevel pinion　　Normal IP bevel pinion

Aknowledgement

The authors express cordial thanks to the JSME Gear Committee RC-268, Toyota Motor Co. and Komatsu Ltd. for their cooperation to work out the development of IP-bevel gears for practical usage.

References

[1] A.Kubo, A.Ueda, "Gear geometry as function of production method - Proposal of Invo-Planar

bevel gear for good productivity –“ , Proc. JSME International Conference on Motion and Power Transmissions, MPT 2017 - Kyoto

Source: © WZL, RWTH Aachen/Ahmad

4th International Conference on Gear Production 2022

3rd Conference day
Wednesday, September 14th, 2022

Measurement technology
Moderation: **Prof. Dr.-Ing. Karsten Stahl,** Full Professor, Institute of Machine Elements, Director, Gear Research Center (FZG), Technical University of Munich (TUM), Garching, Germany

09:30 High speed measurement of hardness distribution with X-ray diffraction

- Converting method from measured FWHM of X-ray diffraction to hardness distribution for all kind of ferric material
- Easy and highspeed contact free measurement of hardness distribution and examples of the measurement for machine parts

Prof. h. c. Dr.-Ing. Aizoh Kubo, General Manager, Dr.-Ing Masahiro Nagae, Research Member, Institute for Applied Sciences, Kyoto, Japan

High-speed measurement of hardness distribution with X-ray diffraction

A. Kubo, RIAS (Research Institute for Applied Sciences);
M. Nagae, RIAS Kyoto 606-8202 Japan;

Abstract

The high-speed hardness measurement using X-ray diffraction to make hardness map and Debye-ring analysis to know more detailed information about steel quality are introduced. To discuss the usability of this method, following examples of the measurement are shown: (1) uniformity of the matrix of market steel, (2) comparison of the hardness deduced from indentation making and that from X-ray diffraction, (3) influence of local difference of grinding and polishing condition of tooth flank on the hardness distribution over the flank, (4) change of surface hardness and residual stresses of heavily used gear teeth and of endurance tested rollers. By evaluating heterogeneous state of hardness distribution and that of uneven 3D form deviation of Debye-ring, we have the impression that this technique can well be used to check the steel and heat treatment quality of gears.

1. Introduction

It is well known that the FWHM (full width at half maximum) of the X-ray diffraction has strong correlation with the hardness of steel. Recently in Japan a very fast measuring technique of FWHM is developed as hardness map maker (refer to HMM). The speed of the measurement is ca.10 sec. for making a FWHM curve along 40mm line and ca.8 minutes to figure 25x95 mm map of FWHM distribution. The working distance of this contact free measurement is 22 mm from the X-ray radiating tip to the target surface, and we can measure e.g. the tooth flank hardness of a gear without cutting the target object into test specimen (refer to TP) and the mirror polishing of the objective surface is not necessary. The measurement of the tooth flank hardness of a gear as its actual usable state is possible as shown below in this paper. This measuring apparatus is already well used in some Japanese industry to examine the uniformity of the matrix of the steel they purchased, e.g. for finding segregation of alloy elements and to find local defect of the steel material, and also for checking the heat treatment quality and for finding grinding burn. Main reason of this industrial usage is that this measurement is very stable: We have not yet experienced any grumpy behavior often experienced by such measurement as those using Barkhausen noise analysis.

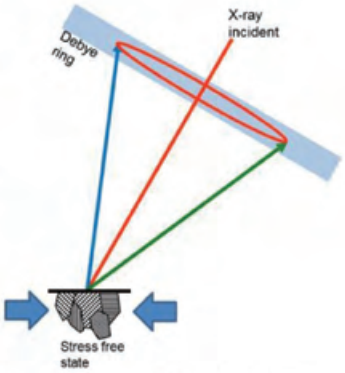

Fig.1 X-ray diffraction and Debye ring

2. Measuring apparatus

We have developed two different kinds of apparatus: one is HMM that based on composite analog and numerical data processing. The other is detailed analyzer of Debye ring based on full numerical data processing (refer to DRA). DRA is the improved model of residual stress measurer to evaluate the deformation of ferrite crystal after cos(α) method of X-ray diffraction analysis. The usability of this apparatus is already reported at the VDI Int'l Gear Conf. 2015 [1]. The DRA needs ca.1 min. to measure one point with using a X-ray spot diameter ϕ 2mm. This measuring speed of DRA is more than 30 times faster than conventional X-ray residual stress measurer of sin(α) principle.

The target items of Debye ring analysis are: 1. Residual compressive/tensile stress, 2. Residual shear stress, 3. FWHM of the Debye ring in many cross-sections, 4. 3D form and asymmetricity of the Debye ring

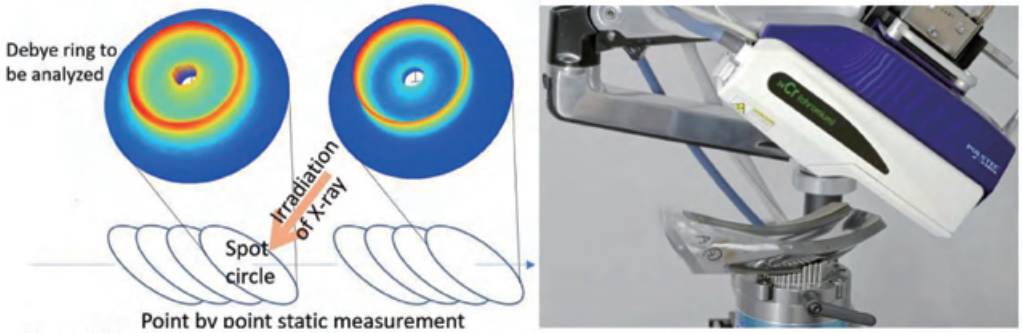

Fig.2 Measurement of DRA

HMM measures the intensity of moving Debye ring in a diagonal cross section with 4 photo sensors. The cross-sectional forms of the Debye ring in its each 360 degree angle cut is often not the same, especially in a case of troublesome steel material, and the analysis of the diffracted X-ray is usually carried out with the average curve of each cross-sectional form of the Debye ring. But it is not the case of HMM. When the 3D form of objective Debye ring is not of a perfect symmetrical crater form, e.g. when mountain height of a crater is up and down around the ring, the measured FWHM becomes therefore different from e.g. that of the DRA. The measuring speed of HMM is 10mm/sec under 100μm interval of data sampling using X-ray spot diameter ϕ 3mm. This speed of HMM is more than 1000 times faster than the speed of DRA, but it measures only FWHM value. When we use X-ray spot diameter of ϕ 1mm, the measuring speed should be decreased to 1mm/sec. for obtaining detailed data.

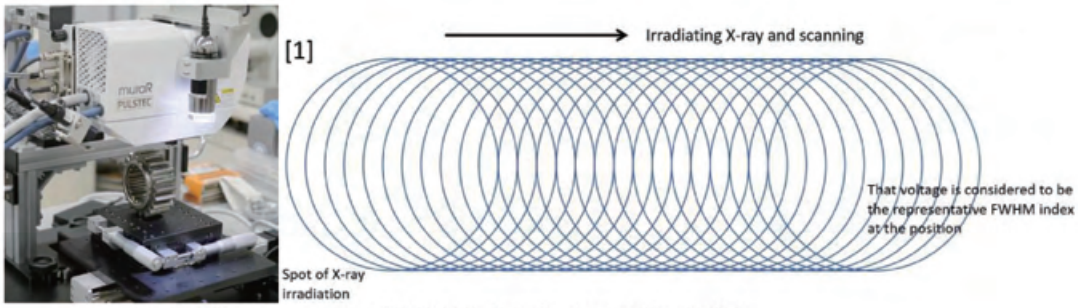

Fig.3 Measurement of FWHM distribution with HMM

The setup of HMM and data sampling procedure is shown in Fig.3. At each sampling point, the average value of the FWHM is transformed into electric voltage Vout and this is taken as the representative FWHM index at the center position of sampled area.

3. Transformation from FWHM to hardness

The FWHM index Vout obtained must be transformed to the hardness value HVmr, that is the Vickers' hardenss value estimated from Vout. This transforming relation changes as function of e.g. carbon %, kind of alloy elements etc. of the steel composition of the TP. It is therefore necessary to make the transforming relation for each kind of material to be measured. If a man works on this matter after normal honest way, the work will never come to the end. I do not want to be involved in such difficult and labor-intensive work. I empoly therefore following way: We measure at first Vickers' hardness with normal indentation making hardness measuring apparatus. That is described as HV[2] in Fig4. We measure also Vout[1] value in Fig4 with HMM at the same place on the same target material. The Vout[1] value is then taken as abscissa and the HV[2] as ordinate in Fig5. One point is then defined in the relation. When we let the corresponding line in Fig.4 move along measuring path, we get the requested relational curve as shown in Fig.5. This procedure is OK in principle, but to work out this job, large labor is still needed and it is not welcome.

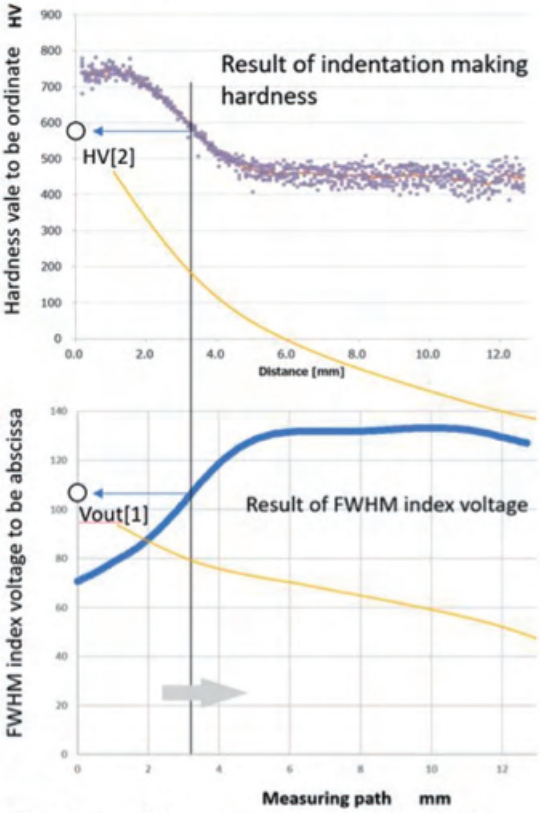

Fig.4 Fvt and Vickers'hardness on the same material

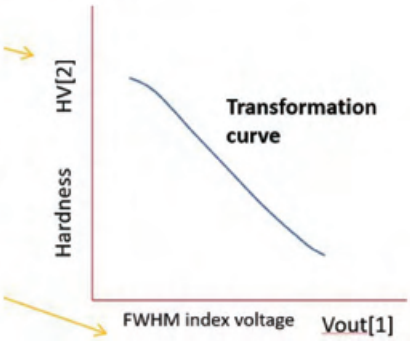

Fig.5 Generation of transforming relation

Fig.6 shows a rough approximating method: this method gives an approximate correspondence between the indentation making hardness HV and the X-ray hardness HVmr, say within 30HV accuracy. To obtain such simplified transforming curve, we need at least two points of coordinate of (indentation making HV vs. Vout output value): they are point 2 and point 4 in Fig.6. The point 2 should be selected as almost hardest value and the point 4 as almost softest value of the target material. From

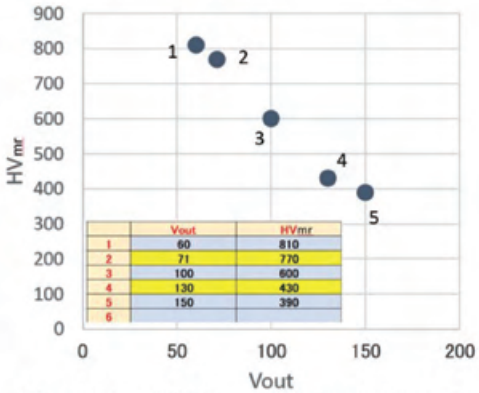

Fig. 6 Simplified method for making the transformation curve

our xperience of many measured results, we know emperically that the form of the transformation curve remains resemble: in the middle part of the curve, the relation is almost linear and we put point 3 between points 2 and 4 to keep this linear relation. In the harder HVmr region, the relation becomes a little bit softer than the extrapolated central line and we assume point 1 at left-low side over the point 2 along the extrapolated linear relation. In the softer HVmr region, the relation becomes a little bit harder than the extrapolated linear relation and we assume point 5 at right-upper side over the point 4. We then obtain an transformation curve from Vout to HVmr, whose region between the point 2 to the point 4 is usually used for the transformation.

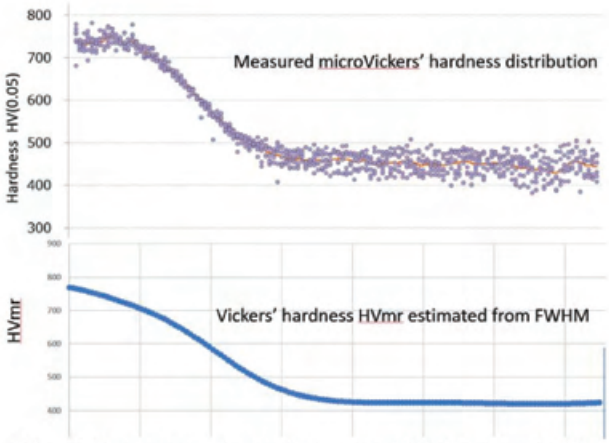

Fig. 7 Correspondence between HV(0.05) and HVmr

The hardness of a TP from a case carburized and hardened big bevel gear tooth of 18CrNiMo7-6 steel was measured: the Vickers' hardeness with 50grf loading with multiple indentation making apparatus[3] and the hardness HVmr is compared with those HV(0.05) as shown in Fig.7. The FWHM measurement was workd out this time with rather larger X-ray spot of diameter ϕ3mm, the state of HVmr corresponds satisfactory with the average curve of HV(0.05) and we consider that the HVmr measured is almost OK for industrial purpose.

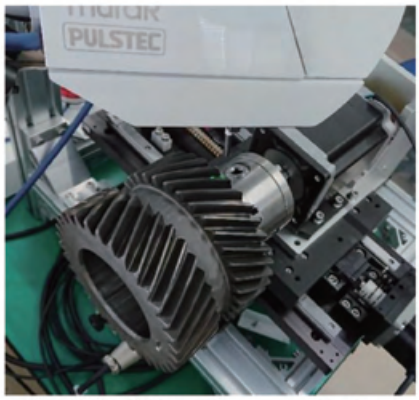

Fig. 8 HMM measurement of double helical gear

4. Example of HVmr map with HMM measurement

As shown in Fig.8, tooth flank measurement of double helical gear for air craft usage is the next example: to measure the HVmr distribution over whole the tooth

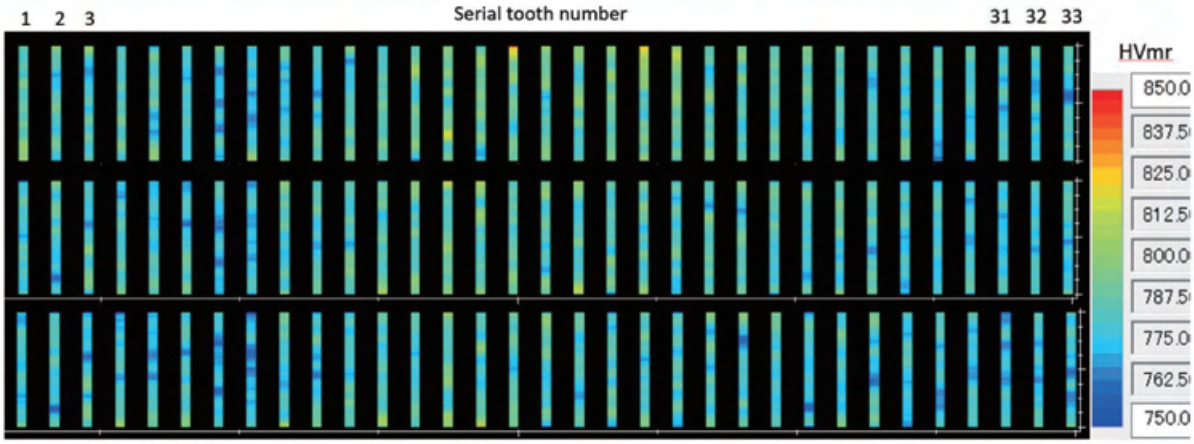

Fig. 9 Reproductability check of 3 times HMM measurement of whole 33 teeth

flanks, we set X-ray incident angle to 45 deg. The Vout to HVmr transformation curve must be newly made for this special measuring condition. To ensure the measuring accuracy, reproductability of the measurement was checked: Fig.9. shows the rsult. After measuring 33 teeth, shown as one raw in Fig.9, the TP gear was demounted and then mounted again for the next measurement. Such procedure repeated 3 times. Each small figure shows the state of hardness HVmr of each tooth flank of the gear. The state of macroscopic HVmr distribution over each tooth flank does not differ much by each measurement and we admitt the reproductability of HMM measurement is OK.

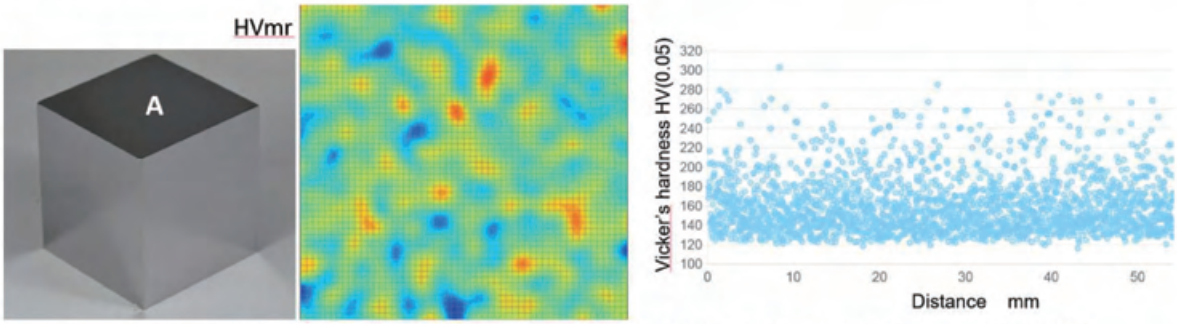

Fig.10 Scattering of hardness of center part of SCM420 steel bar TP, HVmr and HV(0.05)

A test specimen of ca.60x60x60mm cubic block made from the central part of ϕ260 bar of SCM420 steel was measured with HMM using X-ray spot ϕ3mm. The result is shown in Fig.10. On the right side in the figure, indentation making hardness HV(0.05) along mid line on the A-face of the TP is shown. The HVmr map shows a heterogeneous state of steel matrix, that is typical quality usually found in the center of big bar or billet of steel purchased.

5. Endurance tested gear teeth

We measured HVmr of tooth flank of a planet gear for land construction vehicle. This gear was endurance tested on bench and only one side of tooth flank was used. The hardness HVmr of the back flank remains therefore as maiden state. Fig.12 compares the state of hardness HVmr of the endurance tested tooth flank with that of the not-used back flank. The run of HVmr curve along tooth width shows,

Fig.11 HMM measurement of a planet gear

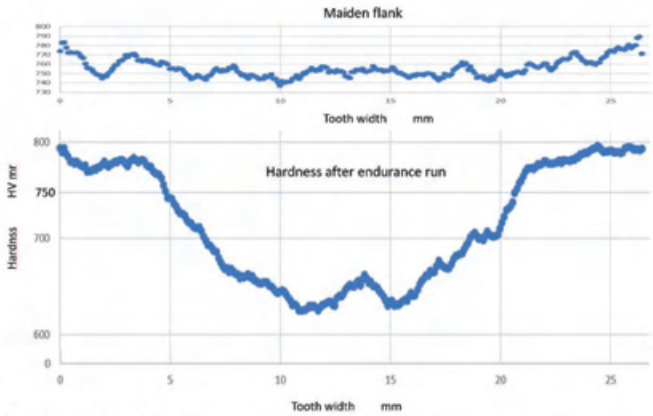

Fig.12 Change of tooth flank hardness due to heavy run

that the hardness at the middle of tooth width of endurance tested flank decreases. The tooth flank has a micro-form correction of lead crowning and the load distribution in the middle of tooth width was high. The hardness decreases there in a same figure as load distribution. The

hardness reduction comes surely from high temperature induced there during the operation.

Next example shows how the HVmr curve changes in the axial direction of the TP by the contact bending fatigue test[2]. The shape of the TP is resemble to rotation-bending TP for fatigue durability test, see Fig.13. The TP was of case carburized, hardened and ground SCM420 and the diameter of test part is ϕ10mm. To minimize the TP deformation during the endurance test, the test part of the TP is supported with two projected parts of backup roller and in the middle of that supporting position, loading disc presses the TP to carry out the contact fatigue test. The nominal contact stress given is 3GPa and considerable spalling occurred after 10^7 rolling cycles.

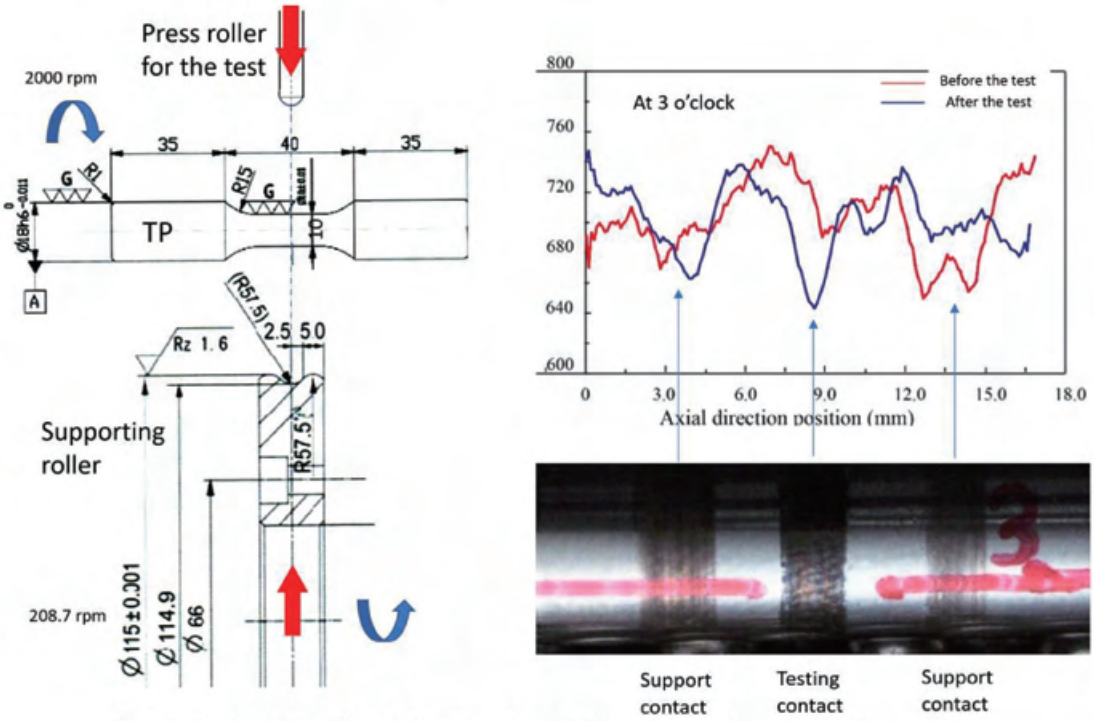

Fig.13 Contact bending fatigue test and HVmr change by contact fatigued bar

When we consider the cross section of the TP as a clock face, spalling occurred at 7 o'clock 30 minute position. Fig.13 shows the state of HVmr at 3 o'clock position, at which no spalling failure occurred. The maiden TP before the test has already some waving distribution of hardness from 650 to 750HVmr. This means, the preparation to such case carburized, hardened and ground TP is not easy to keep its hardness uniform. After the contact fatigue test, the hardness of the TP surface between the contacting points becomes higher, because of the work-hardening induced by bending and shearing deformation, but the hardness under contacting region becomes lower due to the high temperature induced by slipping, elastic deformation and debris crashing during the contact fatigue endurance run.

Fig.14 shows HVmr map of dedendum and addendum of concave tooth flank of big bevel pinion after heavy loaded run. The yellow rectangles in the figure are the region of the measurement. On the lower position of the dedendum at the beginning point of tooth contact, considerable damage due to trochoidal interference is observed. The tooth flank hardness

HVmr there decreases, surely due to the high surface temperature induced by the heat generation during the trochoidal interference.

Along the black line on this tooth flank in Fig.14, the changing state of FWHM, of residual shear stress and of residual compressive stress are analyzed by DRA measurement, cf.Fig.15. In the trochoidal interference groove made on the lowest position of the dedendum during the endurance run, the hardness drops. The direction of residual shear distortion changes in the middle of the interference groove. The deepest position of the residual compressive stress exists in the direction somewhat toward the pitch point in comparison with the deepest position of the residual shear stress and of FWHM.

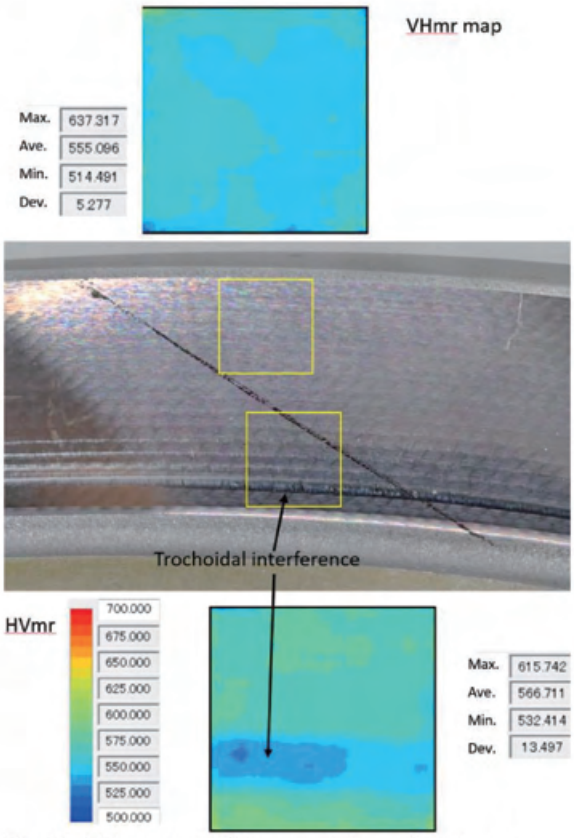

Fig.14 HVmr map of bevel pinion after heavy loaded run

Over whole the tooth flank, the magnitude of the residual shear stress gradually decreases from tooth root to tooth tip. The increasing state of enveloping stressed volume[4] of tooth flank material from dedendum toward addendum can have some relation to this phenomenon, where the enveloping stressed volume means the effective volume of tooth flank material that transmit power or load. The residual compressive stress of the loaded tooth flank remains almost constant from dedendum to addendum. The FWHM, therefore the tooth flank hardness, also remains almost constant from dedendum to addendum.

Fig.16 compares the hardness values, one from the DRA and the other from the HMM i.e. HVmr. The quantitative reliability of HVmr receives considerably big influence from the transformation curve from Vout to VHmr, but the qualitative behavior remains without receiving

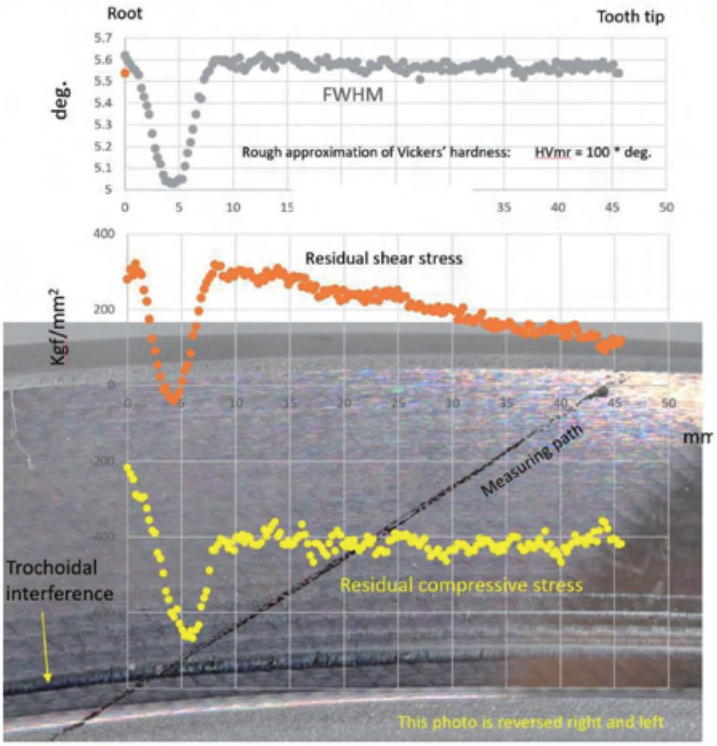

Fig.15 Residual stresses and FWHM of DRA measurement from root to tip (Same tooth flank of Fig.14)

that influence.

After the heavy loaded run of bevel gears, the tooth flank is machined to peeled off the skin by ca.200μm with hard milling. We refer here this retouched tooth to A[4] and not-retouched tooth to A[3], that is of Fig.15. Comparing A[3] with A[4], Fig.17 shows how the state of ferrite crystal deformation of the load carried concave tooth flank differed at ca.8μm depth and at ca.200μm depth from the surface. The dedendum tooth flank at the beginning point of tooth contact is strongly worn by trochoidal interference through the heavy loaded run. The scattering of the FWHM, i.e. hardness scattering, of the loaded surface is somewhat smaller than that of the subsurface. In very near the loaded skin, the scattering of residual deformation of ferrite lattice may be averaged by strong stress repetition during the loaded run. The tooth flank hardness scarcely changes, save in the groove of trochoidal interference. The residual shear stress, i.e. deformation of ferrite crystal, of tooth flank also hardly changes by loaded run. The residual compressive stress of the loaded surface increases slightly by loaded run. Perhaps it is an effect of work-hardening.

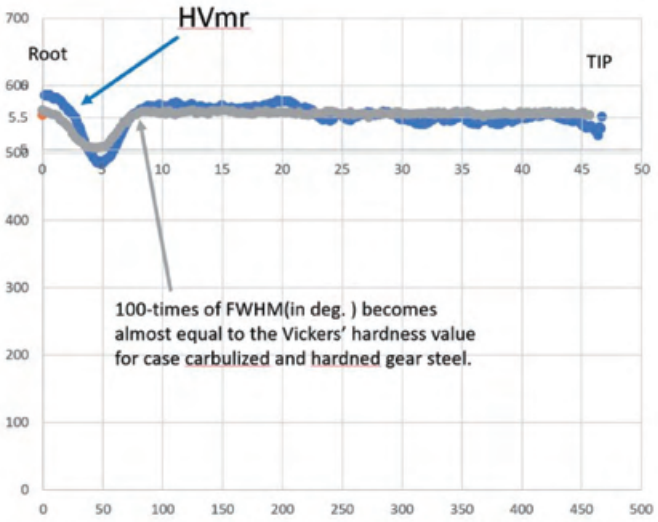

Fig. 16 Comparison of hardness value, of DRA and HMM

The convex tooth flank of this bevel gear carries the load in somewhat different fashion from that of the concave tooth flank. The load distribution concentrates rather strongly to the addendum. The tooth tip edge is plastically deformed and strongly worn due to the trochoidal interference at the disengagement of tooth meshing. The state of ferrite crystal deformation of this tooth flank at ca.8μm depth is compared with that at ca.200μm depth from the surface, Fig.18. The tooth flank hardness at 200μm subsurface is somewhat lower than the loaded surface of 8μm depth. The peeling-off of loaded skin reduces the

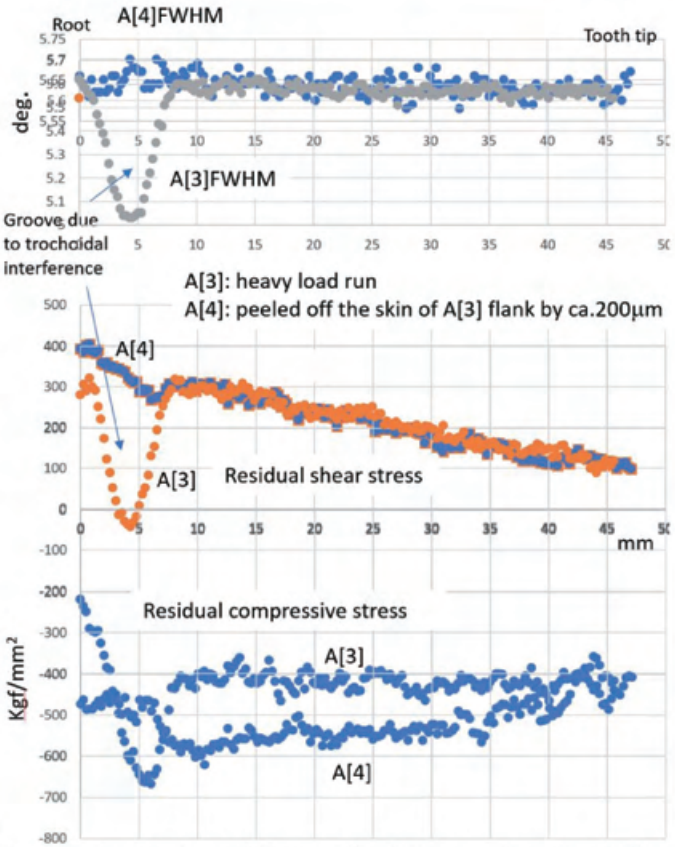

Fig.17 Comparison of the residual stress state near surface and of ca.200μm depth of loaded concave tooth flank

effective case depth of carburized and hardened tooth flank and this could be the cause of the reduction of residual compressive stress. The tooth form near the tip is strongly dropped by wear and plastic deformation due to the trochoidal interference. Strong plastic deformation of ferrite crystal occurred also in the material of 200μm subsurface.

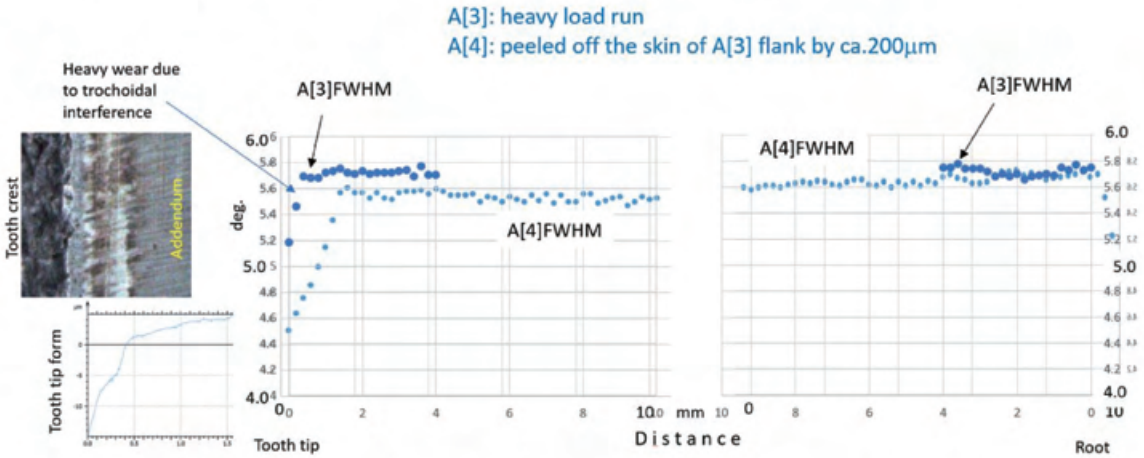

Fig.18 Comparison of the state of FWHM near the surface and that of ca.200μm depth of convex loaded tooth flank

Fig.19 compares the residual compressive stress of the same convex tooth flank whose tooth tip is strongly worn by trochoidal interference. By peeling-off 200μm material from the surface, the changing state of the residual stress shows that the tooth flank material near tooth tip strongly plastically deformed and the material there is work-hardened to raise the compressive residual stress value (larger minus value). On the dedendum tooth flank, the enveloping stressed volume[4] of surface material is smaller than that of tooth middle or of addendum, and the surface temperature there increased. The residual compressive stress there was then released and the residual stress value of A[3] curve moves upward.

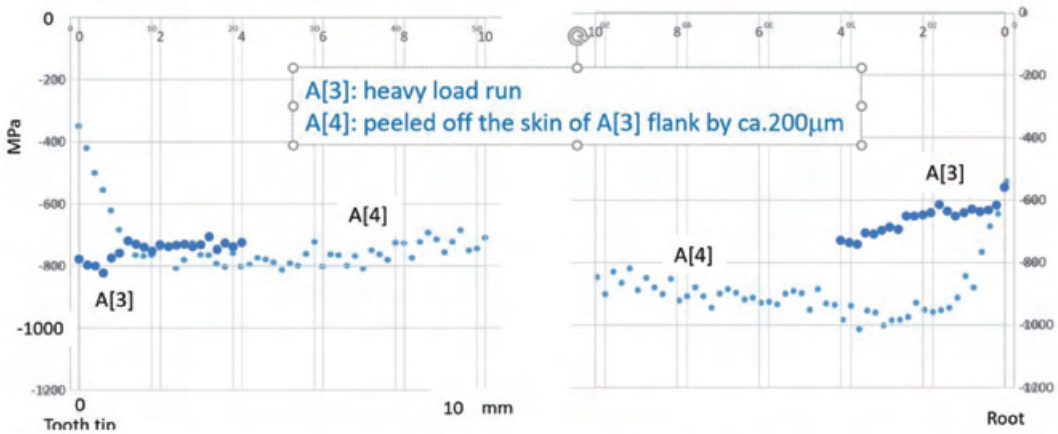

Fig.19 Comparison of the state of residual compressive stress near the surface and that of ca.200μm depth of convex loaded tooth flank

6. Tooth grinding and polishing

Several involute spur gears of m=6, PA=20deg., b=15mm and Z=21 were prepared from SCM420 steel and case carburized and hardened. Those gears were then ground with worm-form grinder to very high accuracy grade. Some gears were then polished with elastic polishing tool of the same kind of worm-form. Fig.20 shows the outlook of the tooth flanks and the surface roughness in the tooth lead

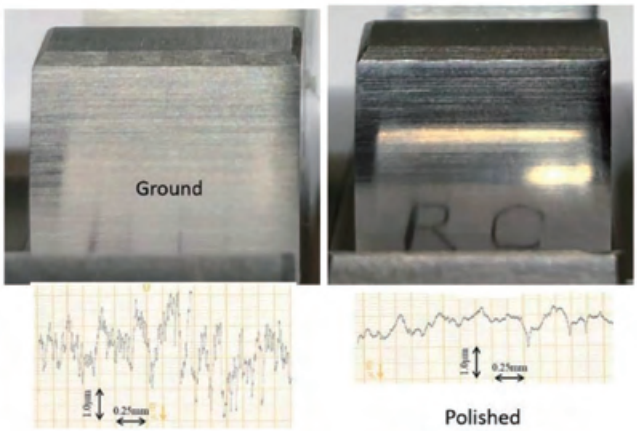

Fig.20 Ground gear and polished gear with spiral tool

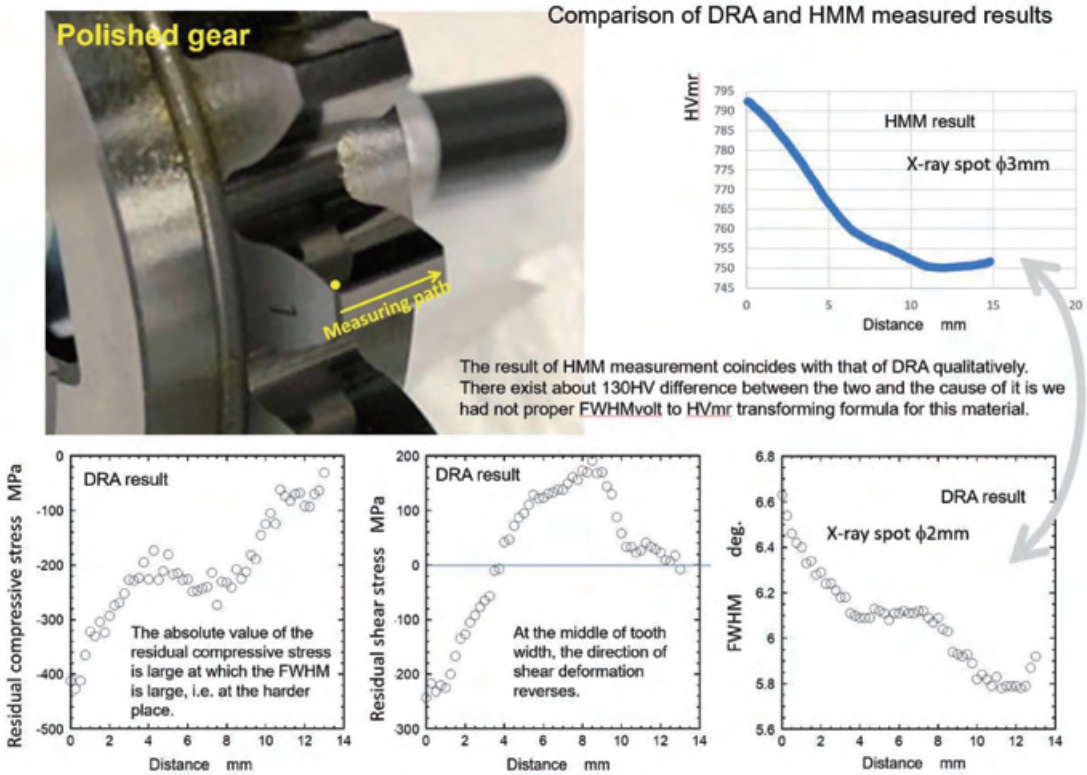

Fig.21 Measured result of DRA and HVmr

direction. The state of ferrite crystal deformation of the tooth flanks was then measured in the lead direction. Fig.21 compares the result of DRA measurement with HVmr. In the rightmost column, the FWHM of DRA is compared with HVmr. In detail there is some difference between the two, but the macroscopic behavior looks resemble. All the items of the measured data shows, they are not constant over the tooth face width direction. This is a fairly big discrepancy from our today's common sense about gear grinding/polishing: Our common sense is, that the state of residual stress and hardness over whole the ground tooth flank does not variates.

Fig.22 compares the state of FWHM of ground and polished tooth flanks. We have the experience that the relation between Vickers' hardness and FWHM of DRA measurement is roughly "10 times of the FWHM in degree is almost equal to HV". In the figure, there exists

about 130HV difference between the result of HMM and of DRA measurement. The cause of this difference is, that we had not proper transforming relation from Vout to HVmr for this material. The qualitative behavior, e.g. the rank in elevation of the HVmr curves, though coincides well with that of DRA .

The overall results of DRA and HVmr show, that the hardness of right and left tooth flank is somewhat different and the hardness of right flank is lower than that of left flank. When we compare the hardness of ground tooth flank and of polished tooth flank, the hardness of ground tooth flank is somewhat higher than that of polished tooth flank. The frictional heat generation on tooth flank at the polishing could be higher than that of the grinding. This is because, the cutting capability of grinding grains is different between grinding and polishing and it changes as functions of cutting edge condition of grinding grains and geometrical contact state of the tool to tooth flank. It changes in the direction along tooth width as grinding/polishing proceeds. The frictional heat generation at polishing receives more delicate influence from these factors than the case of grinding. In the case of polishing, FWHM value is highest at the inlet region (left side of Fig.22) of polishing tool and it decreases gradually to the outlet position of the polishing work, where the polishing tool rubs the tooth flank somewhat strongly. This situation suggests that the heat generation on the polished flank becomes larger in this direction.

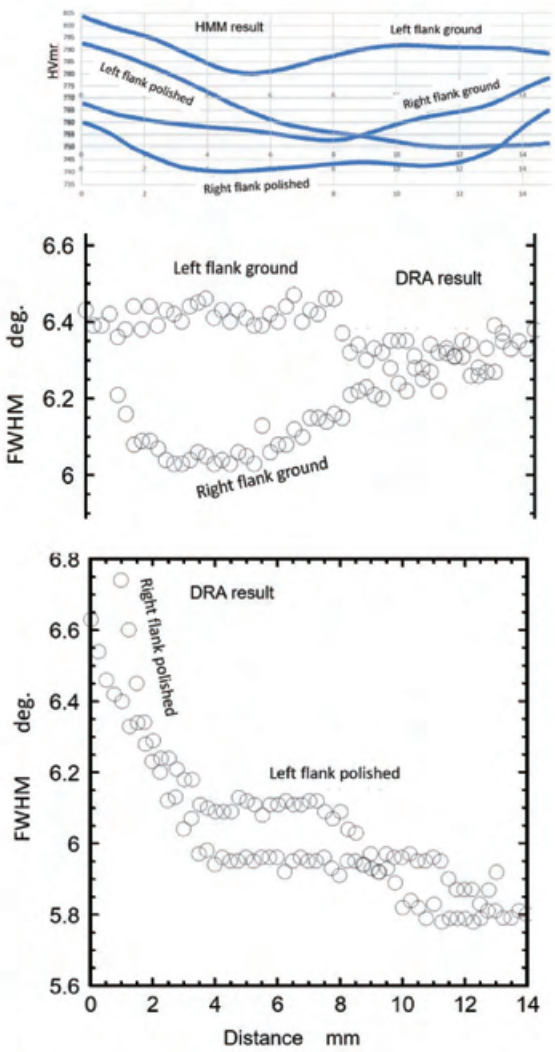

Fig.22 FWHM of ground and polished tooth flank

7. Conclusions

1. To evaluate the qualitative state of hardness distribution over considerable wide area of material surface, hardness map maker HMM was developed. Thanks to its high measuring speed, easiness to prepare the objective specimen, easy measuring operation and the satisfactory accuracy of the measured result, this apparatus can be used to find the problems of material, heat treatment quality and grinding burn.

2. By improving the residual stress measurer of cos(α) method of X-ray diffraction, Debye ring analyzer DRA was developed. This apparatus measures the objective specimen in detail to view the state of deformation of ferrite crystal inside steel and iron material: i.e. the

distribution of residual compressive/tensile stress, of residual shear stress, of FWHM of the Debye ring in different cross sections and of 3D form deviation of the Debye ring.

3. Some measured result of heavy load carried steel parts showed, that the hardness of stressed region becomes harder due to work-hardening effect and the hardness under contact becomes softer due to high temperature induced there during the operation.
4. When gear teeth experiences trochoidal interference during the operation, i.e. strong contact of tooth tip edge to the low meshing limit of dedendum, the hardness of that part of the dedendum and the corresponding tooth tip drops and the residual stress strongly changes.
5. Measured tooth flank hardness of ground gear and polished gear showed, that the tooth flank hardness is not uniform over whole the tooth flank. Perhaps this is because the geometrical working condition between grinding/polishing tool and objective tooth flank differs at each local place on tooth flank to be ground or polished.

References

[1] A.Kubo, T.Sasaki, “Fast and versatile measurement of residual stress and hardness of gear and shaft materials “ , Proc. VDI International Conference on gears, October 2015, Garching, Germany

[2] A.Kubo, S.Matsumoto, T.H.Hou, I.Moriwaki, M.Nakamura, “Contact Bending Fatigue test of gear material against failure due to tribo-cause to fatal subsurface crack propagation”, Proc. VDI International Conference on gears, October 2013, Garching, Germany

[3] A.Kubo, M.Nagae, K.Kawaski, “Japanese standardization for gear steel qualification via evaluation of HV-scattering”, Proc. VDI International Conference on gears, September 2019, Garching, Germany

[4] A.Kubo, “Influence of stressed volume of tooth flank on the surface durability “ , Proc. VDI International Conference on gears, September 2019, Garching, Germany

特別研究員による成果

銀被覆ビスマス系および実用超電導線材の機械的および電磁的特性の評価

特別研究員　長村光造
受託先名：住友電気工業株式会社

1. 目的：銀被覆ビスマス系線材および実用超電導線材とそれらの応用製品の改良のため製品の製作過程および使用環境で想定される様々な条件における機械特性および電磁気的特性を評価する。

2. 成果：本年度は、テープの臨界電流の曲げ歪依存性を平曲げ法および縦曲げ法により調べた。曲げ直径が小さくなると臨界電流が劣化し始めるが、その原因について材料組織学的な観点から考察した。

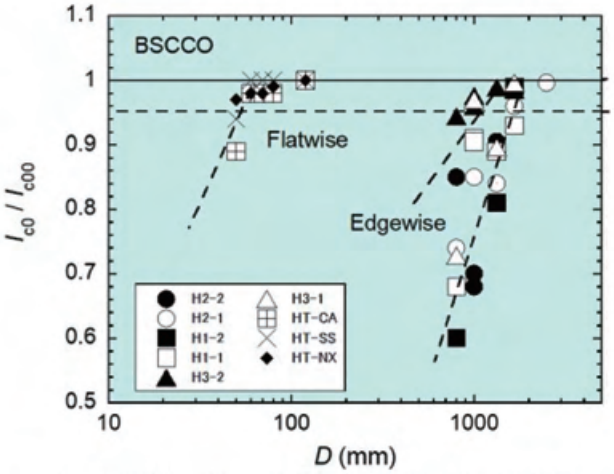

図１　規格化された臨界電流の曲げ直径依存性

図１に示したように平曲げでは 50㎜，縦曲げでは 1200ｍｍ程度で劣化が始まる。曲げによる劣化は(1)曲げる方向、(2)材料の違い、(3)積層構造、厚さ等のテープの幾何学的構造等の要因で曲げ依存性が異なる。検討の結果、曲げにより超電導相に発生する歪量はマトリックスと接する外周部で最大となり、この歪量と臨界電流の変化によい相関が見出された。

3. 成果の公表

1) K.Osamura, S.Yamade and T.Kato, “Degradation Due to Flatwise and Edgewise Bending on Critical Current of BSCCO Tapes”, IEEE Transactions on Applied Superconductivity, 32(2022)8400405, DOI：10.1109/TASC.2022.3153752

2) 長村光造，町屋修太郎，山根昇悟；“臨界電流の曲げ歪依存性測定方法の改善について”，2022 春 低温工学・超電導学会講演概要集 2A-a04
3) 長村光造，町屋修太郎，山根昇悟；“高温超電導テープの臨界電流の限界曲げ歪の評価”，2022 秋 低温工学・超電導学会講演概要集 3B-p07

報告書作成日　令和５年４月７日

IEC 国際標準化

特別研究員　長村光造
受託先名：IEC/TC90 国内技術委員会

１．目的

実用超電導線材の超電導特性測定技術および超電導線材の分類に関する国際標準の制定

２．成果

本年度も超電導技術に関する IEC-TC90 国際および国内専門委員会の技術委員会委員、ワーキングループ WG2(臨界電流測定)，WG5(常温引張試験)および WG13(超電導線材料)のグループリーダーとして国際標準作成の取りまとめを行った。2022. Nov. 1 に San Francisco で開催された国際 WG5 会議の概要を報告する。

CHAIRPERSONS: K Osamura and H-S Shin

PARTICIPANTS: Hyung-Seop Shin, Yifei Zhang, Gen Nishijima, Noriko Chikumoto, Yoshimitsu Hishinuma, Jun Fujikami, Kozo Osamura, Yuichi Yamada, Steven Fleshler,
Yue Zhao, Cees Thieme, Arnoud Allais (12)

PROCEEDINGS

1. Report of the last meeting on May 28, 2022, on-line

2. Maintenance of published standards

Four IEC standards of RT tensile test method have been maintained for Nb-Ti, Nb_3Sn, BSCCO and REBCO wires.

3. Discussion

3.1 Tensile test method at cryogenic temperature

As reported from Germany committee, the present low temperature tensile test method has been already proposed to IEC-NWIP.

3.2 Tensile load dependence of I_c

Proposal of Int-RRT on the HTS superconductors through critical current measurement under tensile load has been updated.

3.3 RT tensile test of MgB_2 wires

The tensile test method of MgB_2 wires was proposed from Japan. A tentative schedule has been explained for Inter RRT,

3.4 Report of WG5 activity in China

The activity of research groups led by Lanzhou University was introduced. RRT has been conducted on the test method of delamination strength of REBCO tapes in China.

報告書作成日　令和 5 年 4 月 7 日

永久磁石材料の高性能化
高保持力化指針構築

研究種別：基盤研究

特別研究員　松浦　裕

1. 目的

永久磁石の磁化反転プロセスを明らかにするとともに磁石特性の改善の方法について探索を行う。

2. 成果

(1) これまでの各種Nd-Fe-B焼結磁石およびフェライト磁石の保磁力の配向度依存性および角度依存性から得られた結果のまとめを行った。

(2) (1)の磁気測定からNd-Fe-B焼結磁石とフェライト磁石の磁化反転過程は同じプロセスが進行することが明らかとなった。

(3) $(Sm, Ce)_2(Co, Fe, Cu, Zr)_{17}$型磁石のXMCD観察結果から得られた保磁力と、磁気測定から得られた保磁力の相関について、検討を行った。

3. 成果の公表

(1) 保磁力の配向度依存性から導かれるNd-Fe-B焼結磁石およびフェライト磁石の保磁力メカニズム

日本ボンド磁性材料協会技術例会

口頭発表（令和4年5月20日 online）

(2) 磁気測定から導かれるNd-Fe-B焼結磁石およびフェライト磁石の磁化反転過程

The magnetization reverse process of Nd-Fe-B sintered and ferrite magnets derived from the magnetic measurement.

電気学会マグネティクス研究会 MAG-22-155

口頭発表（令和4年12月21日　明治大学）

(3) $(Sm,Ce)_2(Co,Fe,Cu,Zr)_{17}$型磁石の磁気測定減磁曲線と軟X線磁気円二色性の平均減磁曲線の相関について

Correlation between the demagnetization curve of the magnetic measurement and the average demagnetization curve of the soft X-ray magnetic circular dichroism in $(Sm, Ce)_2(Co, Fe, Cu, Zr)_{17}$.

日本金属学会春季講演大会（令和５年３月９日　東京大学駒場キャンパス）

(4) 磁気測定から導かれるNd-Fe-B焼結磁石およびフェライト磁石の磁化反転過程
The magnetization reverse process of Nd-Fe-B sintered and ferrite magnets derived from the magnetic measurement.
電気学会マグネティクス研究会 MAG-22-155

上記論文を次頁に掲載する。

報告書作成日　令和５年４月７日

MAG-22-155

磁気測定から導かれる Nd-Fe-B 焼結磁石および フェライト磁石の磁化反転過程

松浦　裕*（公益財団法人　応用科学研究所）

The magnetization reverse process of Nd-Fe-B sintered and ferrite magnets derived from the magnetic measurement

Yutaka Matsuura* (Research Institute for Applied Sciences)

Coercivities of Nd-Fe-B sintered and ferrite magnets are measured with respect to alignment. The measurements imply that multiple grain-related magnetic domain wall motion determines the coercivities of these magnets. Even when the coercivity decreases from 0° in terms of its angular dependence, it decreases from that of isotropic magnets in terms of its alignment dependence, indicating that the magnetic domain wall motion still decides the coercivity. The area angle of the magnetization reversal is calculated from the alignment dependence of coercivity assuming that every grain independently reverses the magnetization. From this calculation, it is inferred that a magnet with a strong alignment behaves like a magnet with weak alignment. The angular dependences of coercivity are obtained using various Gaussian alignment distributions with weak alignment, which are consistent with the angles of the magnetization reversal area for various materials. These dependences agree well with the experimental angular dependencies of coercivities at a small angle. It also explains the decrease in coercivity from 0°. The difference in the alignment and the angular dependences of coercivities for various materials is presumably due to the number of reversed grains forming the cluster. The recoil curves of the Nd–Fe–B sintered and ferrite magnets show a slight decrease in magnetization in the magnetic field region lower than their coercivities. This demagnetization is presumed to be the start of a rapid reduction in magnetization near the coercivities.

キーワード：永久磁石，Nd-Fe-B 焼結磁石 2，フェライト磁石 3，保磁力 4，保磁力メカニズム 5，磁化反転過程 6，
(Keywords, keyword2, keyword3, keyword4, keyword5, keyword6)

1.　はじめに

Nd-Fe-B 焼結磁石およびフェライト磁石に代表される永久磁石はハイブリッド自動車および電気自動車のトラクションモータや自動車用補機モータおよび家電用コンプレッサーモータ等に多く使われるようになってきており、これらモータの省エネルギー化に欠かせない材料となっている。近年、地球温暖化の影響から世界各国の自動車の排出ガス規制は強化されてきており、今後更にこれら磁石の需要は高まるものと推定される。このような状況において永久磁石の特性を改良に関する要求は高まっている。これまで Nd-Fe-B 焼結磁石では保磁力(H_{cJ})が温度とともに減少することから、高温下で使われる磁石の減磁を防ぐ必要があり、室温での H_{cJ}を高くする必要があった。この H_{cJ}を改良するため、焼結後に重希土類を磁石表面に付けた後に熱処理で磁石粒界に拡散させる方法、添加元素を用いて H_{cJ}を上げる方法および粉末粒径を小さくすることで H_{cJ} を上げることが提案され既に商業磁石で使われている。しかし、今後更に磁石特性を上げるためには、この磁石の磁化反転過程を明らかにし、H_{cJ}改良の方向を探ることも重要であると考えられる。ここでは H_{cJ}の配向度依存性と角度依存性および H_{cJ}より低い減磁界領域でのリコイルカーブ等の磁気測定から導かれる磁化反転過程について述べる。

2.　保磁力の角度依存性と配向度依存性

〈2･1〉保磁力の角度依存性

Nd-Fe-B 焼結磁石の微細組織は $Nd_2Fe_{14}B$ 主相結晶粒の周りを Nd-rich 相が取り囲んでおり、粒界三重点で Nd-rich 相、B-rich 相および Nd 酸化物が見られている。Nd-rich 相は Nd-Fe-B 三元系状態図[1]から非磁性相と見做されていたことから、主相結晶粒は磁気的に周りの主相結晶粒から切り離された孤立粒子と考えられていた。この考えを基に、この磁石の H_{cJ} メカニズムは長い間、主相結晶粒 1 個の磁化反転過程について議論が行われてきた。[2],[3],[4],[5] これらの議論の中心は主相結晶粒の磁化が磁化の一斉回転で反転をするのか、それとも磁壁移動で磁化反転するのかであるが、いずれの理論も主相結晶粒の粒界の異方性の弱いところで磁化反転が始まるというものである。磁化一斉回転では粒界の欠陥等の異方性の弱いところで磁化反転の芽が発生す

る（ニュークリエーション）と結晶粒全体の磁化が一斉に回転するというものであり、Stoner-Wohlfarth 理論を修正したものである。一方の磁壁移動モデルも磁化反転磁区が発生する（ニュークリエーション）場所は同じく異方性の弱いところであるが、熱揺らぎ磁気余効の式の中に現れる活性化体積が何らかの過程（Passage）から反転磁区に成長し、磁壁が結晶粒内に侵入することにより磁化反転するというものである。このどちらが実際に起こっているのかを検証する方法として H_{cJ} の角度依存性が用いられてきた。[(2), (5), (6)]

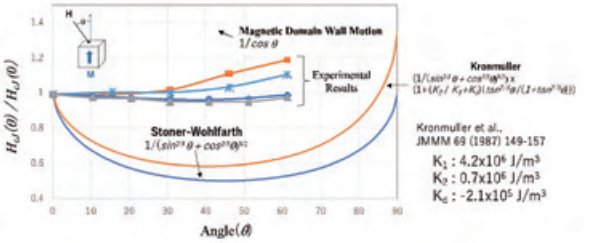

図１　磁化一斉回転および磁壁移動で H_{cJ} が決定されている場合の保磁力の角度依存性と磁気測定から得られる各種磁石の保磁力角度依存性

Fig. 1.　Angular dependence of H_{cJ} for the coherent rotation of magnetism (Stoner-Wohlfarth model and modified model by Krinmuller) and the magnetic domain wall motion, and observed angular dependence of H_{cJ} for various magnets

しかし、図１に示すように実際の磁石の H_{cJ} の角度依存性は磁壁移動（1/cos θ）と磁化一斉回転の間に位置しており、どちらが正しいのかを判断するのは極めて難しい。

〈2･2〉保磁力の配向度依存性

一方、我々は Nd-Fe-B 焼結磁石の配向度(α)を極限まで高めることで残留磁束密度を $Nd_2Fe_{14}B$ の理論値 (1.6T) に近づけるという試みを行い、2005年に磁石特性の世界最高記録を達成した。[(7), (8)] この配向度を上げる試みの中で図２に示すように、α を上げると H_{cJ} は等方性磁石から連続的に減少することが明らかとなった。特に $\alpha > 0.95$ の領域で H_{cJ} は急激に減少し、この領域での H_{cJ} の等方性磁石からの減少割合 (β(%)) を完全配向 ($\alpha = 1$) に外挿した値は、等方性磁石の保磁力に対して30% ほど減少する。[(7), (8), (9)] この H_{cJ} の配向度依存性は Nd-Fe-B 焼結磁石だけでなくフェライト磁石でも観測されており、フェライト磁石も Nd-Fe-B 焼結磁石と同じ磁化反転プロセスが起こっていることが予想される。

この α の向上による β の依存性は、磁化一斉回転で決定される場合は H_{cJ} が増加することが予想されることから、これら磁石では磁化の一斉回転による磁化反転は起こっていない。一方、磁壁移動で H_{cJ} が決定されているとすると $\alpha = 1$ における H_{cJ} は等方性磁石の $1/\sqrt{2}$ となり、これは実験で得られた $\beta = -30$%に近い値であることから、これら磁石では磁壁移動で保磁力が決定されていることを強く示唆している。[(10), (11), (12), (13)]

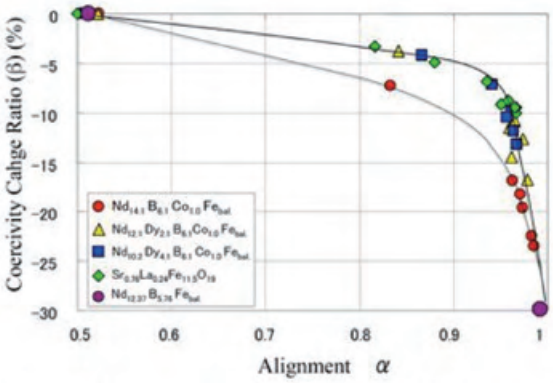

図２　配向度(α)と H_{cJ} の等方性磁石からの減少する割合(β)

Fig. 2.　Relation between alignment and the coercivity change ratio from the isotropic magnets

Nd-Fe-B 焼結磁石の保磁力が磁壁移動で決定されている可能性については、３次元アトムプローブを使った粒界の組成分析からも予想されており、それによると $Nd_2Fe_{14}B$ 主相結晶粒を取り囲む Nd-rich 相の Fe 含有量は平衡状態図から予想される Fe 量より多く、粒界相は磁性相であると考えられるようになってきている。[(14)]

それでは、この磁石を構成している主相結晶粒全てが独立に $1/\cos\theta$ 則に従って磁化反転していると仮定して図２の配向度依存性が得られるのかと言うと、そうではない。Nd-Fe-B 焼結磁石の配向分布は電子線後方散乱(EBSD)からガウス分布と良い一致を示しており、α は配向分布関数を $P(\theta)$ とすると

$$\alpha = \frac{1}{2}\int_0^{\pi/2} P(\theta)\sin 2\theta\, d\theta \qquad (1)$$

で表すことができる。粒子は磁界の配向方向成分により磁化反転すると仮定すると H_{cJ} ($J = 0$)は式(2)で示される

$$J = \frac{1}{2} J_s \left(\int_{\theta_1}^{\pi/2} P(\theta)\sin 2\theta\, d\theta - \int_0^{\theta_1} P(\theta)\sin 2\theta d\theta\right) = 0 \qquad (2)$$

ここで θ_1 を磁化反転領域角度とし、H_{cJ} では 0° から θ_1 まで磁化反転していることを示している。その時の β は θ_1 を用いて

$$\beta = \left(\frac{1}{\sqrt{2}\cos\theta_1} - 1\right) \times 100 \qquad (3)$$

式(1), (3)の α と β を実験の値と比べると α は実験と良く会うのに対して β は実験値と大きく異なっていることが分かった。この結果は、主相結晶粒は独立して磁壁移動により磁化反転しているのではなく、H_{cJ} で磁壁移動により磁化反転粒子の集団(クラスター)を形成していることを示唆している。[(15)]

〈2･3〉保磁力の配向度依存性と角度依存性の相関

これまで Nd-Fe-B 焼結磁石の H_{cJ} の配向度依存性と角度依存性の温度変化についてはあまり知られていないが、その後の検討で大きく変化することが分かってきた。[16], [17], [18] H_{cJ} の配向度依存性は温度の上昇とともに(1), (2)式で求められる曲線に近づいていく。一方で角度依存性は $1/\cos\theta$ の曲線に近づいていくことが分かった。このことから H_{cJ} の配向度依存性と角度依存性はお互いに関係しており、保磁力メカニズムの一側面であることが推定される。

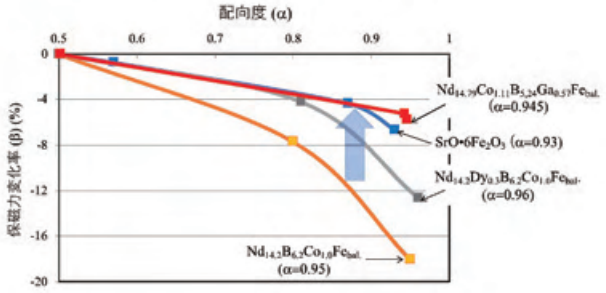

図 3　各種磁石の H_{cJ} の配向度依存性

Fig. 3.　Alignment dependence of H_{cJ} for various magnets

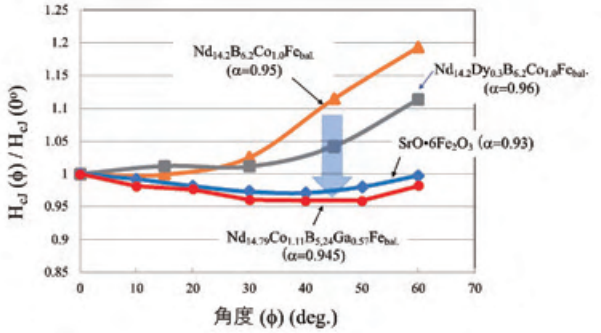

図 4　各種磁石の H_{cJ} の角度依存性

Fig. 4.　Angular dependence of H_{cJ} for various magnets

図３に各種磁石の H_{cJ} の配向度依存性を、図４に保磁力の角度依存性を示している。 H_{cJ} の配向度依存性は全ての磁石で等方性磁石の H_{cJ} から減少しているが、その減少量は組成に因って異なっている。一方、H_{cJ} の配向度依存性と角度依存性は図３、図４の矢印で示しているように連動していることが分かった。図４ではフェライト磁石および Ga 添加 Nd-Fe-B 焼結磁石の H_{cJ} の角度依存性を示しているが、これら磁石の H_{cJ} は角度の増加に従い一旦減少し、その後増加する。このような角度依存性は磁化の一斉回転の特徴とされており、従来の考えであればフェライト磁石および Ga 添加 Nd-Fe-B 焼結磁石の H_{cJ} は磁化一斉回転で決定されているとされる。しかし、これら磁石の H_{cJ} の配向度依存性は等方性磁石から減少していることから、H_{cJ} は磁壁移動で決定されていることを示している。[19], [20] これまで H_{cJ} のメカニズムの検証を H_{cJ} の角度依存性のみを用い行われてきたが、角度依存性だけを使った議論では間違った結論に導かれる可能性がある。したがって、配向度依存性の観点から考察することは欠かせないものと考えられる。

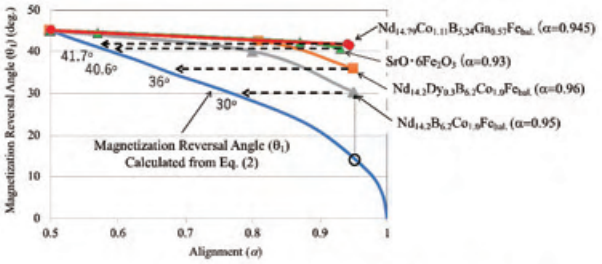

図 5　磁化反転領域角度(θ_I)の配向度依存性

Fig. 5.　Alignment dependence of the magnetization reversed area (θ_I)

H_{cJ} の配向度依存性と角度依存性の相関を求めるために各組成による θ_I の値を式(4)から求め、式(2)から得られた θ_I と比べた。図５はその結果を示している。実際の磁石の θ_I の値は式(2)で求めた同じ配向度の θ_I に比べ大きくなっていることが分かる。これは実際の磁石では全ての粒子が独立に磁化反転した場合に比べて、磁化反転粒子の集団（クラスター）が大きくなっており、あたかも配向度の悪い磁石のように振る舞っていることを示している。またクラスターの大きさは組成や温度によって異なっていると解釈される。これを確かめるため球面三角法を用い異なる θ_I を持つ磁石の H_{cJ} の角度依存性を求め、実験で求めた角度依存性と比較した。[19], [20], [21] 計算で求めた H_{cJ} の角度依存性は配向分布関数($P(\theta)$)として図５から得られた実際の磁石より低い配向度を用いた。

図６は計算から求めた H_{cJ} の角度依存性と実験で得られた角度依存性を比較したものである。計算で求めた H_{cJ} の角度依存性は低角度側で実験結果と良く合っている。また、配向分布関数として用いたガウス分布の標準偏差(σ)を変えていくと、H_{cJ} の角度依存性は0°から下がっていくことも明らかとなった。H_{cJ} の配向度依存性から得られる情報は磁界方向と磁化が平行と場合の情報であり、この情報を用いて角度依存性を議論する場合、当然のことながら低角度側での挙動でしか議論できない。しかしながら、低い配向度を持った配向分布を用い保磁力の角度依存性を求めると、ある配向分布（$\theta_I > 38°$）から 0°以上の角度で H_{cJ} が低下する。こ

の結果は実際の磁石では H_{cJ} 点での磁化反転粒子が形成するクラスターが大きくなることにより、あたかも配向度の低い磁石のように振る舞っているという仮説の正しさを示しているものと推定される。

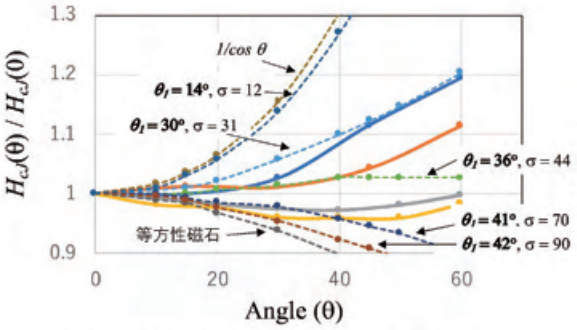

図 6　θ_fから求めた H_{cJ} の角度依存性（破線）と磁気測定結果の比較

Fig. 6.　Comparison of the angular dependence of H_{cJ} calculated from θ_f and the results of the magnetic measurement

〈2･4〉等方性磁石の保磁力の角度依存性について

図５から、高配向度領域で異なる θ_f を持つ磁石であっても、全ての磁石の等方性磁石の θ_f は45°に収束することを示している。このことは全ての磁石は等方性磁石であれば、図６に示した H_{cJ} の角度依存性をを示し、0° から保磁力が減少することが推定される。このような予想に基づき測定した等方性磁石の H_{cJ} の角度依存性を図７に示す。

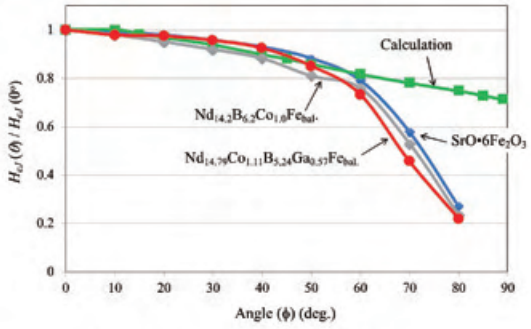

図７　等方性磁石の H_{cJ} の角度依存性

Fig. 7.　Angular dependence of H_{cJ} for various isotropic magnets

図から全ての磁石で H_{cJ} は 0° から減少しおよそ 60° 付近まで計算値と良く合っていることが分かった。このことはこれら磁石の H_{cJ} が磁壁移動により説明できることを強く示唆している。[19], [20], [22]

3.　リコイル特性について

ここまで Nd-Fe-B 焼結磁石およびフェライト磁石について H_{cJ} の配向度依存性および角度依存性を用いて、これら磁石の H_{cJ} は複数の粒子が関係した磁壁移動により保磁力が決定されることを議論してきた。しかし、それでは、これら磁石において磁壁あるいは磁化反転した結晶粒は H_{cJ} より低い磁界で既に存在しているのかと言うことが問題となる。

Nd-Fe-B 焼結磁石では表層の結晶粒は加工により粒界相である Nd-rich 層が無くなっている事から、表層の磁石では H_{cJ} が失われていることが想定されており、実際に低磁界領域で僅かな磁化の減少が観測される。しかし、Nd-Fe-B 焼結磁石およびフェライト磁石では減磁曲線の角形性が良く。加工劣化に見られる低磁界での磁化減少以外での減磁は無いものと見られており、磁化反転が起こるニュークリエーション磁界は磁化の急激な変化が起こり始める磁界とされてきた。[23]

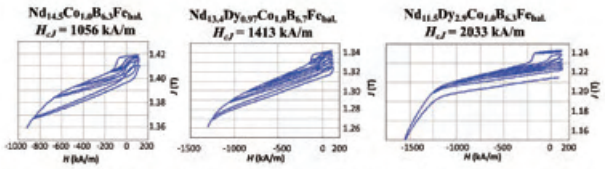

図８　H_{cJ} より低い減磁界領域での各種 Nd-Fe-B 焼結磁石のリコイルカーブ

Fig. 8.　Recoil curve for various Nd-Fe-B sintered magnets in lower demagnetization field than H_{cJ}

図８は H_{cJ} の異なる磁石について、H_{cJ} より低い磁界でリコイルカーブを調べた結果を示している。磁界 0 kOe に近いところで見られる磁化の減少は加工による表面劣化層から来る磁化の減少である。いずれの磁石も磁化は減磁界が大きくなるにつれて連続的に減少しており、加工劣化とは異なる減磁が起こっていることが確認された。[15] この減磁が磁石表面のみで起こっている現象であるのか、それとも磁石全体で起こっているのか確かめるため磁石体積(V)と表面積(S)が異なる磁石を用い、低い減磁界両機での磁化の減少を調べたところ、S/V に依存しない減磁が観測された。このことから、この減磁が表面で起こる現象ではなく、磁石全体で生じている減磁であることが分かった。[15]

軟 X 線磁気円二色性(XMCD)による磁化反転過程の観察から、弱い減磁界領域では離散的な結晶粒の磁化反転が観測されており、これがリコイルカーブで見られる減磁と対応しているのではないかと考えられる。 XMCD から、減磁界が大きくなると、この離散的に磁化反転した結晶粒に隣接した結晶の磁化反転によりクラスターが発生する様子も

確認されている。

4. まとめ

Nd-Fe-B 焼結磁石およびフェライト磁石の磁気測定、特に H_{cJ}の配向度依存性から、この磁石の H_{cJ}は複数の粒子が関係した磁壁移動で決定されていることが導かれる。

これまでは H_{cJ}の角度依存性を用いて H_{cJ}のメカニズムが議論されてきた。しかし、H_{cJ}が 0° から減少する場合でも、H_{cJ}の配向度依存性は等方性磁石から減少することから、このような場合でも H_{cJ}は磁壁移動で決定されている。配向度依存性と角度依存性は互いに連動しており、これら配向度依存性と角度依存性は H_{cJ} メカニズムの一側面を見ているものと考えられる。

全ての粒子が独立して磁化反転するとして配向度の依存性から求めた磁化反転領域角度から、高い配向度を有する磁石ではあたかも配向度が低い磁石のように振る舞っていることが推定される。

磁化反転領域角度と一致する、低い配向度の配向分布を用いて求めた H_{cJ} の角度依存性は実験から得られる角度依存性と低角度側で良い一致を示す。また保磁力が 0° から減少する現象も説明できるように思われる。

この H_{cJ} の角度依存性の違いは H_{cJ} でのクラスターの大きさから生じているものと推定される。

Nd-Fe-B 焼結磁石およびフェライト磁石のリコイルカーブから H_{cJ} より低い磁界領域で僅かな磁化の減少が観測されており、この低い減磁界で起こる減磁が起点となって H_{cJ} 近傍で急激な磁化の減少を引き起こしているものと推定される

文　　献

(1) Yutaka Matsuura, Satoshi Hirosawa, Hitoshi Yamamoto, Setsuo Fujimura, Masato Sagawa, Kozo Osamura: "Phase diagram of Nd-Fe-B ternary system", Jpn. J. Appl. Phys., Vol. 24(8), L635- L637 (1985)

(2) H. Kronmuller, K. -D. Durst, G. Martinek: "Angular dependence of the coercivity field in sintered $Fe_{77}Nd_{15}B_8$ magnets", J. Magn. Magn. Mater., 69, 149-157 (1987)

(3) D. Givord, P. Tenaud, T. Viadieu: "Coercivity mechanism in ferrite and rare earth transition metal sintered magnets (SmCo5, Nd-Fe-B)", IEEE Trans. Magn., 24, 921-1923 (1988)

(4) D. Givord, M. Rossignol, V. M.T.S. Barthem:" The Physics of coercivity" J. Magn. Magn Mater., 258-259, 1-5 (2003)

(5) S. Bance, H. Oezelt, T. Schrefl, G. Ciuta, N. M.Dempsy, D. Givord, M. Winklhofer, G. Hrkac, G. Zimanyi, O. Gutfleisch, T. G. Woodcock, T. Shoji, M. Yano, A. Kato, A. Manabe: "Influence of defect thickness on the angular dependence of coercivity in rare-earth permanent magnets", Appl. Phys. Lett., 104, 182408 (2014)

(6) D. Givord, P. Tenaud, T.Vidieu: "Angular dependence of coercivity in sintered magnets", J. Magn. Magn, Mate., 72, 247-252 (1988)

(7) 播本大佑、松浦裕：「超高性能 Nd-Fe-B 焼結磁石の開発」，日立金属技報」，Vol.23,　pp. 69-72 (2007)

(8) Y. Matsuura: "Recent development of Nd-Fe-B sintered magnets and their applications", J. Magn. Magn. Mater. 303, 343-347(2006)

(9) 播本大佑、松浦裕、細川誠一：「Nd-Fe-B 磁石特性に及ぼす結晶配向の影響」, J. Jpn. Soc. Powder Powder Metallurgy, Vol.53, No.3 号 pp.282-284 (2006)

(10) Y. Matsuura: "Coercive force mechanism derived from the relation between $Nd_2Fe_{14}B$ grain alignment and coercive force decrease ratio in NdFeB sintered magnets", The 22nd International Workshop on Rare-Earth Permanent Magnets and their Applications, 147-150 (2012)

(11) 松浦裕："NdFeB 焼結磁石の保磁力減少率の配向度依存性と保磁力メカニズム ", 金属, Vol. 83 No. 2, pp 28-32 (pp 120-124) (2013)

(12) Y. Matsuura, J. Hoshijima, R. Ishii: "Relation between Nd2Fe14B grain alignment and coercive force decrease ration in NdFeB sintered magnets", J. Magn. Magn. Mater., 336, 88-92 (2013)

(13) 北井伸之, 松浦裕, 石井倫太郎, 棗田充俊, 星島順："Nd-Fe-B 焼結磁石の保磁力減少率の配向度依存性と保磁力メカニズム", 日立金属技報, Vol. 30, 20-27 (2014)

(14) H. Sepehri-Amin, T. Ohkubo, T. Shima, K. Hono: "Grain boundary and interface chemistry of an Nd-Fe-B-based sintered magnet", Acta Mater., 60, 819-830 (2012)

(15) Y. Matsuura, N. Kitai, R. Ishii, M. Natsumeda, J. Hoshijima: "Recoil properties and coercive force decrease ratio in NdFeB sintered magnets", J. Magn. Magn. Mater., 346, 113-117 (2013)

(16) Y. Matsuura, N. Kitai, M. Natsumeda, R. Ishii, J. Hoshijima: "Temperature dependence of coercive force decrease ratio in Nd-Fe-B sintered magnets", The 22nd International Workshop on Rare-Earth Permanent Magnets and their Applications", 128-1-3 (2014)

(17) Y. Matsuura, N. Kitai, R. Ishii, M. Natsumeda, J. Hoshijima, F. Kuniyoshi: "Temperature properties of the alignment dependence of coercive force decrease ratio and the angular dependence of coercive force in Nd-Fe-B sintered magnets", J. Magn. Magn. Mater., 398, 246-252 (2016)

(18) Y. Matsuura, N. Kitai, S. Hosokawa, J. Hoshijima: "Relation between the alignment dependence of coercive force decrease ratio and the angular dependence of coercive force of ferrite magnets", J. Magn. Magn. Mater., 411, 1-6 (2016)

(19) Y. Matsuura: "Coercivity mechanism of Sr O·$6Fe_2O_3$ ferrite magnets", IEEE Trans. Magn., 54 (11), 2101405 (2018)

(20) Y. Matsuura, T. Nakamura, K. Ishigami, K. Kajiwara, K. Sumitani, R. Tamura, M. Nagae, K. Osamura: "Coercivity mechanism of Ga-doped Nd-Fe-B sintered magnets", IEEE Trans. Magn., 55 (12), 5100606 (2019)

(21) Y. Matsuura, T. Nakamura, K. Sumitani, K. Kajiwara, R. Tamura, K. Osamura: "Angular dependence of coercivity derived from alignment dependence of coercivity in Nd-Fe-B sintered magnets", AIP advances, 8 (1) (2018)

(22) Y. Matsuura, T. Nakamura, K. Sumitani, K. Kajiwara, R. Tamura, K. osamura, "Angular dependence of coercivity in isotropically aligned Nd-Fe-B sintered magnets", AIP Advances, 8(5) 056236 (2018)

(23) F. Cebollada, M. F. Rossignol, D. Givord: "Angular dependence of coercivity in Nd-Fe-B sintered magnets; Proof that coherent rotation is not involved", Phys. Rev. B, 52, 13511-13518 (1995)

共同研究員による成果

安定性向上に資する分散電源システムの制御系設計

共同研究員　舟木　剛
大阪大学大学院工学研究科教授

受託先名：株式会社ダイヘン

１．目的

配電系統に連系する分散型電源の電力システムは、太陽電池や風車が発電した直流を系統連系インバータによって、交流に変換し、グリッドに同期投入する。電力システムが正常である場合、系統連系インバータが位相同期回路 PLL より系統電圧の位相を検出し、電流制御を行うことで、系統と負荷の両方に電力を供給する。一方で、短絡、地絡などの事故が発生した場合は、系統連系インバータが事故を検出し、系統から負荷への電力供給を即時停止させる。この時、事故が発生した系統を切り離して、独立運転モードに移行することで、負荷電圧を一定に維持して電力を供給する。また、系統が正常な状態に戻るときは、インバータを独立運転モードから系統連系モードに移行することで、系統に再接続して運用する。インバータは系統連系モードと独立運転モードの二制御モード間を移行し続けることで、災害時でも負荷に電力供給を安定的に続ける。しかし、モードの切り替え時は、系統電圧や周波数などが急激に変動し、配電系統内の機器に影響を与える。そこで本研究では、系統連系モードから独立運転モードに、または、独立運転モードから系統連系モードに移行する際に生じる急激な電圧・電流・周波数変動を抑制するシームレスな制御方法について検討を行う。

２．成果

図 1 に実験系の全体構成と図 2 開発した短絡事故時の系統連系モードと独立運転モードの切り替えの制御アルゴリズムを示す。

図 3 は短絡事故時における電力：50%、インバータ電力:50%）と独立運転(系統電力：0%、インバータ電力:100%）間の切り替えのシミュレーション結果である。接続点(PCC）で系統側の ab 相を短絡させ、事故の発生を模擬する。PCC でのインバータ線間電圧 Vab−inv(黒線)、系統の線間電圧 Vab−grid(橙線)、a 相のインバータ出力電流 Ia−inv(赤線）と a 相の負荷電流 Ia−load(青線)を示している。図より短絡故障発生前の系統連系中(t =−4～0ms）は、インバータが負荷に電力を 50%供給しているため、インバータの出力電流が 0.5 p.u.となっている。t1 において短絡事故が発生し、インバータの出力電圧が 0p.u. になり、インバータの出力電流が −1.8 p.u.まで増加した。系統連系インバータが系統周期の半サイクルで、短絡事故を検出しており、t=0 ms で短絡事故した系統を切り離し、系統連系モードから独立運転モードに移行している。インバータの線間電圧が元の電圧に復帰すると、インバータの出力電流が 1 p.u. に増加した。短絡事故した系統は正常な状態で復帰させるため、故障除去後 PLL を再起動し、インバータと系統電圧の位相を同期させた後に並列することで、t3 で系統連系モードに戻った。系統連系に戻った瞬間、インバータの出力電流は 0.5 p.u. となり、提案アルゴリズムで事故前後のシームレスな運用が可能であることを示した。

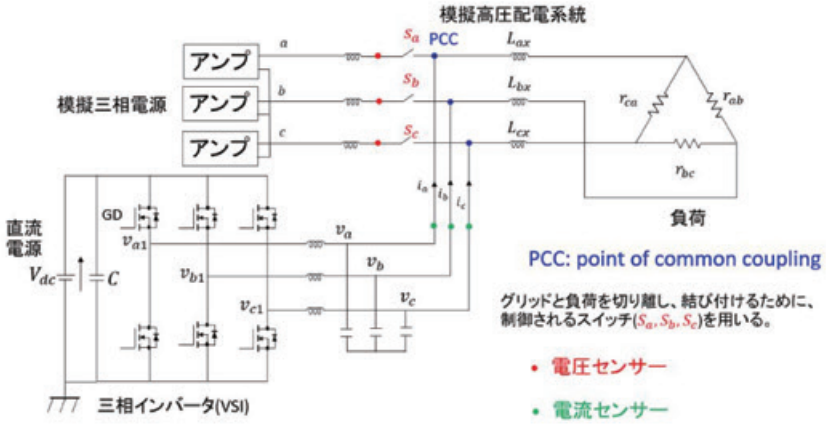

図１　実験系の全体構成

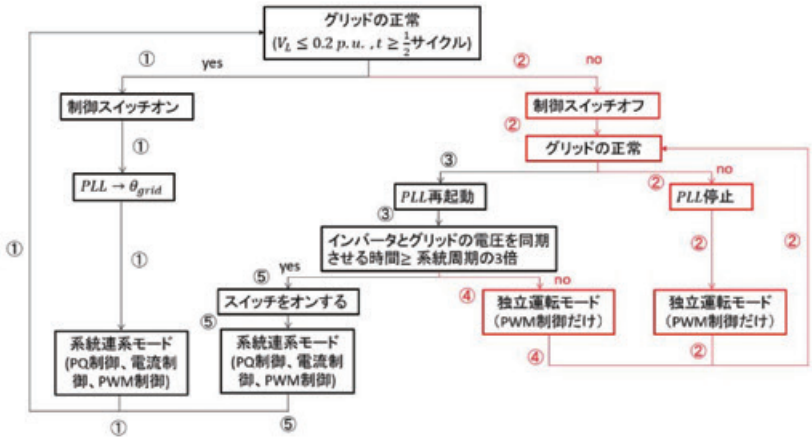

図２　短絡事故時の系統連系モードと独立運転モードの切り替えの制御アルゴリズム

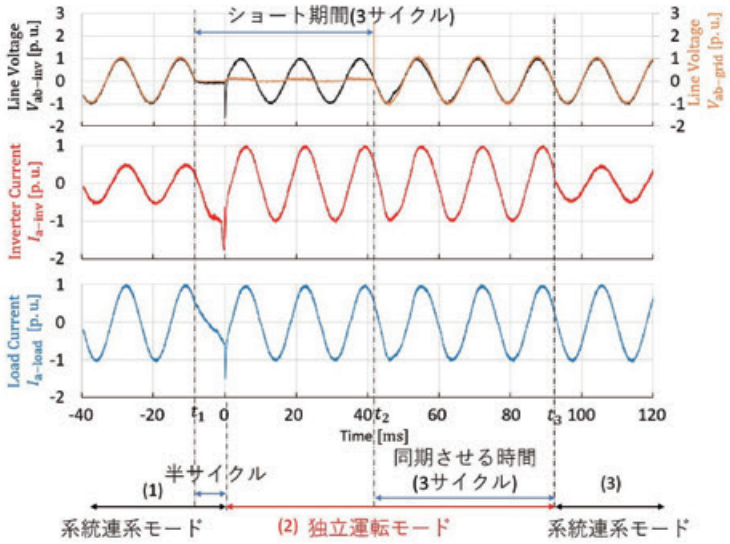

図３　配インバータ線間電圧、グリッドの線間電圧、インバータ出力電流と負荷電流時間応答

３．成果の公表

今年度はなし

報告書作成日　令和５年３月 17 日

エネルギーマネジメントにおける制御アルゴリズム開発

共同研究員　太田　快人[1]　　平田　研二[2]
[1]京都大学大学院情報学研究科教授
[2]富山大学工学部教授

受託先名：株式会社ダイヘン

1. 目的

太陽光発電システムの連系容量の増加に対して電力系統の安定運用を確保するための発電設備や蓄電池設備の制御、電力需要群に対する消費電力の制御に対してアルゴリズムを開発し検証することを目的としている。

2. 成果

蓄電池をともなった太陽光発電設備の発電電力や蓄電量、電力需要群に対する消費電力を分散協調制御する仮想発電所に対する制御方法を考察している。これらの制御問題に対して価格提示分散アルゴリズムを提案し、シミュレーションならびに模擬電源装置による実験を行っている。さらに実験結果から問題点を抽出し、手法の改良を継続している。

3. 成果の公表

(1) 寺崎隼斗，平田研二，阿久津 彗，北村高嗣，大堀彰大，服部将之，太田快人，
価格提示を利用した仮想発電所における階層分散型制御の実機実験に関する考察，
第 10 回 制御部門マルチシンポジウム，2A8-2，2023.

報告書作成日　令和５年４月５日

イオン拡散抵抗の測定評価と解析

共同研究員　安部武志
京都大学大学院工学研究科教授

受託先名：日産化学株式会社

１．目的

リチウムイオン電池に代表される高性能蓄電池は、従来の蓄電池と比べて高いエネルギー密度が特徴であるが、電気自動車や定置用蓄電システムなどの高い要求水準に応えるためには、電池のさらなる高容量化が必要である。そこで、工学的なアプローチとして、電極活物質の塗工量を増やし、緻密化を目指す取り組みがなされている。電極厚みが増し、活物質間に隙間がなくなると、電解液の浸透が困難になり、稼働イオンであるリチウムイオンの輸送が困難になる。そのため、電池の相反する特性である「高容量化」と「高出力化」を両立するために、電極内の空隙構造とイオン拡散（輸送）抵抗の関係を正確に調べる必要がある。しかし、電極の伝導度測定からでは、電極内をイオンと電子の両方が移動するため、イオン拡散抵抗のみの情報を抽出することは難しく、測定手法の確立が求められる。そこで、電極の集電体に多数の穴を開けた銅箔を利用し、その上に活物質からなる合剤電極を作製することで、イオン電流のみが電極を貫通する測定系を構築し、電極のイオン拡散抵抗を測定することを試みた。

今年度も黒鉛活物質とバインダーからなる合剤電極を作製し、四端子法を用いた電気化学インピーダンス測定から多孔質電極のイオン拡散抵抗を評価する手法の確立を目指した。

２．成果

黒鉛活物質は比較的ソフトな材料であり、電極形成時に圧力を加えることで変形し、活物質層の密度を変化させることができる。このことを利用して、本年度も引き続き、電極密度の異なる合剤電極を作製した。電極密度を高くすると電極内のイオン拡散抵抗に起因する電気化学インピーダンスの半円弧が大きくなることが分かった。高い電極密度を有する電極は、活物質どうしが密に詰まり、電解液が浸透する空隙が少なくなる。そのため、電極を貫通するイオン拡散抵抗が高くなったと考えられる。また、イオン拡散抵抗は単調に増加することなく、ある電極密度の閾値以上で急激に増加することが分かった。このことは、イオン拡散に必要な空隙を保ちつつ、高容量化を見込める電極密度の最適値があることを示唆している。今後は、活物質の表面性状がイオン拡散に与える影響を詳細に明らかにすることを予定している。

３．成果の公表

今年度はなし

報告書作成日　令和５年４月７日

リチウムイオン電池用ポリマー電解質材料の開発

共同研究員　安部武志
京都大学大学院工学研究科教授

受託先名：トヨタ自動車株式会社

１．目的

スマートフォンなどの小型電子機器からプラグインハイブリッド車や定置用蓄電システムなどの大型機器に至るまで、リチウムイオン電池は幅広く利用されている。特に、近年では電気自動車の普及にともなって充電時間の短縮が強く求められており、電池の入出力特性の改善が急務である。一般に、リチウムイオン電池では有機電解液が電解質として用いられているが、電池の高い作動電位、すなわち正極での酸化力、負極での還元力によって電極上での電解液の分解が引き起こされる。そこで、リチウムイオン電池の安全性を飛躍的に向上させるために、ポリマー電解質が注目されている。ポリマー電解質は、ベースとなるポリマーとリチウムイオンを含む電解質塩で構成され、骨格となるポリマーをどのように設計するか、に関して様々な検討がなされてきた。本研究では、近年開発が大きく進んでいる誘電率の高いポリマーを用いて、新たなポリマー電解質を設計し、そのイオン伝導特性や輸率、電位窓の電解質としての特性と電極との親和性を抽出することを目的とする。

２．成果

新たに開発したポリマーは従来から使われているポリ（ビニリデンフルオリド-co-ヘキサフルオロプロピレン）（PVDF-HFP）と比べて、高い誘電率を有することがわかった。誘電率は電解質塩の乖離促進に大きく寄与すると考えられる。解離性の高いリチウム塩であるリチウムビス（トリフルオロメタンスルホニル）アミド（LiTFSA）やリチウムビス（フルオロスルホニル）アミド（LiFSA）は比較的溶解度が高く、良好なイオン伝導特性が得られることが明らかになった。今後は、ほかのリチウム塩を用いたポリマー電解質を作製し、さらなる電気化学的解析を進める予定である。

３．成果の公表

今年度はなし

報告書作成日　令和５年４月７日

水中の有害有機物を高効率に分解可能な光触媒材料の開発

共同研究員　阿部 竜
京都大学大学院工学研究科教授

受託先名：カルテック株式会社

１．目的

水中に存在する有害な有機物（におい成分や菌類）は、陸上養殖や植物工場等をはじめとして様々な業界で問題となっており、それらの効率的な無害化手法の開発が強く求められている。本研究では、このような有害有機物や菌類を、太陽光下あるいは安価な発光ダイオード（LED）光源等を用いて効率良く分解、もしくは無害化できる光触媒材料の開発を目的とする。阿部研究室では、これまでに太陽光水素製造の実現を目的として、可視光応答型光触媒を種々開発してきた。また、室内の可視光を利用できる酸化タングステン（WO_3）系光触媒を世界で初めて開発し、従来の酸化チタン（TiO_2）系との複合化による分解活性向上および対象物質拡大にも成功している。本研究では、これまでに開発してきた光触媒材料および知見を活かしながら、これまで対象としていなかった水中の有害物質の分解および無害化に対して必要な光触媒材料の物性などを明らかにし、それに基づいて高活性な光触媒体の開発と水浄化システムの実用化を目指した研究を進める。

２．成果

本年度は、これまで気相有機物分解に用いてきた各種光触媒体を、液相有機物分解へと応用し、両者における差異などの知見を得て、さらなる高性能化の指針を打ち立てることを第一の目的とした。光触媒として「1. 市販可視光応答化 TiO_2」、当研究室で開発した「2. 表面修飾型 WO_3」および「3. TiO_2-WO_3 複合型」の３種を主に用い、種々の有機物存在下において、波長 420 nm 以上の可視光を照射し、生成する二酸化炭素（CO_2）を定量した。一例として、酢酸をモデル物質として気相反応と液相反応を行った結果を示す。2 と 3 の WO_3 系光触媒は、気相および液相いずれにおいても 1 の市販 TiO_2 系より高い CO_2 生成速度を示し、WO_3 の優位性が示された。しかし、WO_3 系では気相反応に比べて液相反応での CO_2 生成速度が大きく低下しており、比表面積の増大や水中における選択的な有機物の吸着特性の付与などが、今後の課題と考えられる。今後は、上記課題の解決を進めるとともに、対象有機物質を体系的に調査することで、水中の有害有機物を高効率に分解可能な光触媒材料の開発を進める予定である。特に、これまで気相反応において芳香族の分解に有効であった TiO_2-WO_3 複合型光触媒が、液相の各種有機物に対してどのような反応特性を示すか、など検討する予定である。

光触媒	初期CO_2生成速度 / μmol h^{-1}	
	液相反応	気相反応
市販可視光応答型TiO_2	2.9	3.1
表面修飾型WO_3	7.7	20.3
TiO_2-WO_3複合型	5.5	16.5

酢酸添加量：1.5 μL (26 μmol)
光源：300 W Xe lamp (λ > 420 nm)

３．成果の公表

今年度はなし

報告書作成日　令和４年４月８日

非線形動力学に基づく計測・制御系の設計

共同研究員　引原隆士
京都大学大学院工学研究科教授

受託先名：寄附研究室

１．目的

システムの非線形特性を利用した新しい計測手法、制御手法を、非線形力学の状態の過渡特性や次元の変化を組み込んだアルゴリズムの開発を行うことを目的としている。

２．成果

2022年度は、1）電力パケット伝送方式のシステム実装（モータ制御、無線電力伝送、ロボット制御）、2）ワイドバンドギャップ半導体パワーデバイスの物理特性を考慮したデジタルアクティブゲートドライバの開発と最適設計、3）配電系統の安全性を考慮した運用アルゴリズムの開発、4）非線形ポテンシャル中の群ロボットのフォーメーション制御アルゴリズムの開発を実施した。それらの成果は３.のリストに示す通りである。

３．成果の公表

1）Shuhei Fukunaga, Hajime Takayama, and Takashi Hikihara, A study on digital active gate driving of DC-DC converter for suppressing switching surge voltage, The 2022 International Power Electronics Conference (IPEC-Himeji 2022 -ECCE Asia-), 19F1-3, Hyogo, Japan, May 15-19, 2022.

2）Yu Shiogai, Alberto Castellazzi, and Takashi Hikihara, Characterrization and switching strategy development for SMP SiC Power Modules, The 2022 International Power Electronics Conference (IPEC-Himeji 2022 -ECCE Asia-), Hyogo, Japan, May15-19, 2022.

3）間宮 崇弘，持山 志宇，引原 隆士，電力パケット伝送システムを用いた無線給電における電力変動の抑制に関する一検討，システム制御情報学会 研究発表講演会，制御応用 114-2 (2022. 5. 18).

4）藤井 俊輔，引原 隆士，可到達集合に基づく配電系統における危険性の数値的評価に関する検討，システム制御情報学会 研究発表講演会，システム理論・応用 115-5 (2022. 5. 18).

5）Hajime Takayama, Shuhei Fukunaga, and Takashi Hikihara, Simulation tool for optimization of digital active gate drive sequence using genetic algorithm, EPE 2022 ECCE Europe, Paper ID: 19, Hannover, Germany (2022.9).

6）Yanran Wang and Takashi Hikihara, Nonlinear external potential curvature estimation by swarm formation: Theory and experiment, 9th IFAC Symposium on Mechatronic

Systems and 16th International Conference on Motion and Vibration Control (MOVIC), Los Angels (2022.9).

7) Hajime Takayama, Shuhei Fukunaga, and Takashi Hikihara, An estimation of load-dependent characteristics of SiC power MOSFETs while active-gate-driving, International Conference on Silicon Carbide and Related Materials (ICSCRM)2022, Tu-P-B.22, Davos, Switzerland (2022.9).

8) 間宮 崇弘，持山 志宇，引原 隆士，複数系間の電力融通にむけた電力パケットの無線伝送に関する一検討，信学会 回路とシステム研究会（2022. 10. 20）.

9) 藤井 俊輔，薄 良彦，引原 隆士，可到達集合に基づく配電系統における電圧変動の危険性評価に関する検討，信学会 非線形問題研究会（2022. 10. 20）.

10) 青木 勇磨，引原 隆士，単方向結合双安定系における外部入力印加時の自励振動波形のモード遷移，信学会 非線形問題研究会（2022. 11. 25）.

11) Hajime Takayama, Shuhei Fukunaka, and Takashi Hikihara, Exhaustive search of digitized gate voltage for SiC MOSFETs, 2022 International Symposium on Nonlinear Theory and its Applications (NOLTA 2022), C2L-B-01 (2022.12).

12) Shiu Mochiyama, A PDM-based strategy for power packet dispatching on shared power line, 2022 International Symposium on Nonlinear Theory and its Applications (NOLTA 2022), C2L-B-02 (2022.12).

13) Ryo Takahashi, Takahiro Mamiya, Shiu Mochiyama, Hamzeh Jaber, Takashi Hikihara, and Alberto Castellazzi, Performance evaluation of discontinuous-PWM Y-Inverter AC motor drive system focusing on a wide range of motor rotation speeds, 2022 International Symposium on Nonlinear Theory and its Applications (NOLTA 2022), C2L-B-05 (2022.12).

14) Shuhei Fukunaga, Hajime Takayama, and Takashi Hikihara, Slew rate control of switching transient for SiC MOSFET in boost converter using digital active gate driver, IET Power Electronics, Volume16, Issue3, Pages 472-482 (19 February 2023).

15) 金本 公平，高山 創，引原 隆士，電圧制御型アクティブゲートドライブにおけるスイッチング特性の分布に関する検討，信学会 総合大会，A-1-4，（2023. 3. 7）.

16) 川染 陸人，持山 志宇，引原 隆士，SR モータ駆動時の電力パケット情報読取りに関する一検討，信学会 総合大会，A-1-5，（2023. 3. 7）.

17) 樋渡 建人，持山 志宇，引原 隆士，電力回生を考慮した電力パケット密度変調に関する一検討，信学会 総合大会，B-9-7，（2023. 3. 10）.

18) 福永 崇平，高山 創，引原 隆士，ダブルパルス試験による事前決定駆動パラメータを用いた電力変換回路の動特性改善，電気学会全国大会，232-C3，（2023. 3. 17）.

報告書作成日　令和５年３月 30 日

令和5年7月印刷・発行
発行：公益財団法人応用科学研究所
〒606-8202 京都市左京区田中大堰町49
TEL 075-701-3164　FAX 075-701-1217
印刷・製本：株式会社北斗プリント社

RIAS®

Since 1917

Research Institute for Applied Sciences